THE JOURNAL OF BIOLOGICAL CHEMISTRY VOL. 282, NO. 4, pp. 2405–2422, January 26, 2007

Expression and Functional Characterization of the Cancer-related Serine Protease, Human Tissue Kallikrein 14*

Received for publication, August 31, 2006 and in revised form, November 14, 2006 Published, JBC Papers in Press, November 16, 2006, DOI 10.1074/jbc.M608348200

Carla A. Borgoño[‡], Iacovos P. Michael[‡], Julie L. V. Shaw[‡], Liu-Ying Luo[‡], Manik C. Ghosh[‡], Antoninus Soosaipillai[‡], Linda Grass[‡], Dionyssios Katsaros[§], and Eleftherios P. Diamandis[‡1]

From the [‡]Department of Pathology and Laboratory Medicine, Mount Sinai Hospital and the Department of Laboratory Medicine and Pathobiology, University of Toronto, Toronto, Ontario M5G 1X5, Canada and the [§]Department of Gynecology, Gynecologic Oncology Unit, University of Turin, Turin 10126, Italy

Human tissue kallikrein 14 (KLK14) is a novel extracellular serine protease. Clinical data link KLK14 expression to several diseases, primarily cancer; however, little is known of its (patho)-physiological role. To functionally characterize KLK14, we expressed and purified recombinant KLK14 in mature and pro-enzyme forms and determined its expression pattern, specificity, regulation, and *in vitro* substrates. By using our novel immunoassay, the normal and/or diseased skin, breast, prostate, and ovary contained the highest concentration of KLK14. Serum KLK14 levels were significantly elevated in prostate cancer patients compared with healthy males. KLK14 displayed trypsin-like specificity with high selectivity for P1-Arg over Lys. KLK14 activity could be regulated as follows: 1) by autolytic cleavage leading to enzymatic inactivation; 2) by the inhibitory serpins α_1-antitrypsin, α_2-antiplasmin, antithrombin III, and α_1-antichymotrypsin with second order rate constants (k_{+2}/K_i) of 49.8, 23.8, 1.48, and 0.224 μM^{-1} min^{-1}, respectively, as well as plasminogen activator inhibitor-1; and 3) by citrate and zinc ions, which exerted stimulatory and inhibitory effects on KLK14 activity, respectively. We also expanded the *in vitro* target repertoire of KLK14 to include collagens I–IV, fibronectin, laminin, kininogen, fibrinogen, plasminogen, vitronectin, and insulin-like growth factor-binding proteins 2 and 3. Our results indicate that KLK14 may be implicated in several facets of tumor progression, including growth, invasion, and angiogenesis, as well as in arthritic disease via deterioration of cartilage. These findings may have clinical implications for the management of cancer and other disorders in which KLK14 activity is elevated.

Proteases include a group of enzymes that catalyze peptide bond hydrolysis. Serine proteases (SP),[2] characterized by the presence of a nucleophilic serine residue at the active site, account for 30% of all proteases within the human degradome (1). Based on structural homology, SP are categorized into 12 clans, the most highly populated being clan PA(S), and are further classified into families that share high sequence similarity (2).

Human tissue kallikreins (KLK, EC 3.4.21) form a subgroup of 15 secreted (chymo)tryptic-like SP within the S1A family of clan PA(S) and are encoded by the largest contiguous cluster of protease genes in the entire genome, located on chromosome 19q13.4 (1, 3, 4). Because KLKs are widely expressed, KLK activity is implicated in an assorted array of normal physiological processes (*e.g.* blood pressure regulation, skin homeostasis, and semen liquefaction) and in the pathobiology of several diseases (*e.g.* cancer, neurodegenerative disorders, and dermatoses) (3–5). Because of the frequent dysregulation of KLK expression in malignancy, KLKs have been intensely studied in terms of their clinical applicability as cancer biomarkers. In addition to human kallikrein 3 (KLK3, also known as prostate-specific antigen (PSA)), the premier biomarker in clinical medicine for prostate cancer (6), most other KLKs have emerged as promising markers of diagnosis, prognosis, prediction of therapeutic response, and monitoring for several cancer types, particularly ovarian carcinoma (5).

Along with seven other KLK genes, human tissue kallikrein gene 14 (*KLK14*) was independently identified in our laboratory by positional candidate cloning in 2001 (7, 8). Subsequent studies demonstrated that the *KLK14* gene is under steroid-hormone regulation (9, 10) and is most highly expressed in the glandular epithelia of the breast (10, 11) and prostate (8, 10) and in the epidermis (*i.e.* stratum granulosum) and appendages (*i.e.* hair follicular epithelium and eccrine sweat glands) of the skin (10, 12, 13). Consequent to its secretion, KLK14 forms a constituent of seminal plasma (10) and sweat (14) and is present in its catalytically active form in the stratum corneum of the skin (13–15). Furthermore, aberrant KLK14 expression has been detected in patients with breast (7, 10, 11, 16), ovarian (7, 9, 10), prostate (7, 17), and testicular (7) cancers and peeling skin syndrome (18), at the tissue and/or serum level. Correlative clinical data have also linked elevated *KLK14* mRNA expression

* The costs of publication of this article were defrayed in part by the payment of page charges. This article must therefore be hereby marked "*advertisement*" in accordance with 18 U.S.C. Section 1734 solely to indicate this fact.

[1] To whom correspondence should be addressed: Dept. of Pathology and Laboratory Medicine, Mount Sinai Hospital, 600 University Ave., Toronto, Ontario M5G 1X5, Canada. Tel.: 416-586-8443; Fax: 416-586-8628; E-mail: ediamandis@mtsinai.on.ca.

[2] The abbreviations used are: SP, serine proteases; ACT, α_1-antichymotrypsin; AP, α_2-antiplasmin; $AS_{4.5}$, angiostatin4.5; ATIII, antithrombin III; BisTris, 2-[bis(2-hydroxyethyl)amino]-2-(hydroxymethyl)propane-1,3-diol; ECM, extracellular matrix; IGFBP, insulin-like growth factor-binding protein; HPLC, high performance liquid chromatography; KLK, kallikrein; LMWK, low molecular weight kininogen; MMP, matrix-metalloprotease; PAI-1, plasminogen activator inhibitor; RSL, reactive site loop; serpin, serine protease inhibitor; MES, 4-morpholineethanesulfonic acid; PSA, prostate-specific antigen; ELISA, enzyme-linked immunosorbent assay; DMEM, Dulbecco's modified Eagle's medium; FBS, fetal bovine serum; AMC, 7-amino-4-methylcoumarin; ACN, acetonitrile; IGF, insulin-like growth factor; Tos, tosyl; Boc, *t*-butoxycarbonyl; Suc, succinyl; AT, α_1-antitrypsin.

with aggressive forms of breast (11, 16) and prostate cancer (17) and with the prognosis of breast (16) and ovarian (9) cancer patients. Thus, KLK14 represents a potential biomarker and therapeutic target for several pathologic conditions.

As with all S1A family SP, KLK14 is synthesized as an inactive precursor or zymogen (herein denoted pro-KLK14), containing a 6-amino acid N-terminal pro-peptide that maintains its latency (7, 8). Proteolytic removal of the pro-peptide at Lys^{24}–Ile^{25} is required to generate active KLK14, a process that may be performed by KLK5 (19). Because of the presence of Asp^{198} in its S1 binding pocket (7, 8), KLK14 is predicted to exert trypsin-like substrate specificity with a preference for basic P1 residues (Schechter and Berger nomenclature (20) is used to describe the interaction between protease subsites (S*n*-S1;S1′–S*n*′) and corresponding substrate residues (P*n*-P1;P1′–P*n*′), where P1–P1′ denotes the scissile bond). However, we (21) and others (19), through the use of phage-display technology and chromogenic substrates, respectively, have recently demonstrated that KLK14 can accommodate both basic (Arg and Lys) and hydrophobic (Tyr) P1 residues at the S1 subsite with a preference for Arg. Hence, KLK14 manifests dual, trypsin-like and chymotrypsin-like, substrate specificity.

To date, putative biological substrates and (patho)physiological roles for KLK14 have been inferred from its expression pattern, substrate specificity, and the known function of co-localized KLKs. Phage-displayed pentapeptide motifs preferred by KLK14 were identified within several intact proteins, including the extracellular matrix (ECM) molecules laminin, collagen type IV, and matrilin-4 (21). The latter may support a role for KLK14 in cancer progression via ECM digestion, particularly in breast, ovarian, and prostate tumors that bear elevated KLK14 levels. Because of its presence and prominent activity in the stratum corneum of the skin (13–15), KLK14 is also implicated in epidermal desquamation (*i.e.* shedding) via degradation of intercellular (corneo)desmosomal adhesion molecules that link adjacent corneocytes (19). More recently, our group has reported that KLK14 may also mediate pleiotropic effects by signaling through proteinase-activated receptors 1, 2, and 4 (22). KLK14 may exercise its functions alone or in a proteolytic cascade pathway, as KLK5 may activate pro-KLK14 and vice versa (19).

Collectively, studies on KLK14 reveal that this novel SP may play important (patho)physiological roles at the main sites of its expression and bears clinical utility. To gain further insights into the biological significance of KLK14 action, this study examines KLK14 expression, specificity, activity against candidate substrates, and several modes of regulation.

EXPERIMENTAL PROCEDURES

Cloning, Expression, and Purification of Recombinant KLK14

Mature KLK14—Mature recombinant KLK14 was produced in the Easyselect™ *Pichia pastoris* expression system (Invitrogen), as described previously (21). Briefly, PCR-amplified *KLK14* cDNA encoding the mature enzyme form of KLK14 (amino acids 25–251 based on GenBank™ accession number AAK48524) was cloned into *P. pastoris* expression vector pPICZαA (Invitrogen) at EcoRI and XbaI restriction enzyme sites between the 5′ promoter and the 3′ terminator of the *AOX1* gene, in-frame with the yeast α-mating factor (for secretion), using standard techniques. The *PmeI*-linearized pPICZαA-*KLK14* construct was transformed into chemically competent *P. pastoris* yeast strains X-33, GS115, and KM71. A stable X-33 transformant was selected, and recombinant KLK14 expression was induced with 1% methanol/day for 6 days at 30 °C in a shaking incubator (250 rpm).

Mature recombinant KLK14 was purified to homogeneity from culture supernatant by a two-step procedure consisting of cation-exchange and affinity chromatography. Typically, 1 liter of culture supernatant was clarified by centrifugation and concentrated 20-fold by positive pressure ultrafiltration in an Amicon™ stirring chamber (Millipore Corporation, Bedford, MA) with a 10-kDa cutoff nitrocellulose membrane (Millipore). The concentrated supernatant was diluted 1:4 in 10 mM MES (pH 5.3) and fractionated on a pre-equilibrated 5-ml cation-exchange HiTrap™ SP HP column (GE Healthcare), with the automated ÁKTA FPLC system (GE Healthcare). Adsorbed KLK14 was eluted with a multistep salt gradient using 1 M KCl in 10 mM MES (pH 5.3) at a flow rate of 3 ml/min as follows: (*a*) continuous linear gradient of 0 – 0.3 M KCl for 17 min, (*b*) maintenance at 0.3 M KCl for 20 min, (*c*) followed by a continuous linear gradient from 0.3–1 M KCl for 50 min. Elution fractions (3 ml) containing KLK14 were identified (as described below), pooled, and concentrated using Biomax-10 Ultrafree®-15 centrifugal filter device (Millipore Corp., Bedford, MA). The concentrated fractions were diluted 1:4 in 100 mM Tris-HCl (pH 7.8) binding buffer and incubated with 1 ml of soybean trypsin inhibitor-agarose beads (Sigma) overnight at 4 °C. The beads were then packed into an Econo-Pac open column (Bio-Rad) and washed three times with binding buffer. KLK14 was eluted with 0.1 M glycine buffer (pH 3.0).

Pro-KLK14—First-strand cDNA synthesis was performed by reverse transcriptase using the Superscript™ preamplification system (Invitrogen) with 2 μg of total human cerebellum RNA (Clontech) as a template. The cDNA encoding prepro-KLK14 (amino acids 1–251 based on GenBank™ accession number AAK48524) was PCR-amplified in a 50-μl reaction mixture containing 1 μl of cerebellum cDNA as a template, 100 ng of primers (forward, 5′ CACC ATG TTC CTC CTG CTG ACA GCA CTT; reverse, 5′ AGA CCA *TCA* TTT GTC CCG CAT CGT TTC CT, containing CACC sequence required for TOPO® cloning (underlined) and the native KLK14 stop codon (italics)), 10 mM Tris-HCl (pH 8.3), 50 mM KCl, 1.5 mM $MgCl_2$, 200 μM deoxynucleoside triphosphates (dNTPs), and 0.75 μl (2.6 units) of Expand Long Template PCR polymerase mix (Roche Diagnostics) on an Eppendorf master cycler (Eppendorf, Westbury, NY). PCR conditions were 94 °C for 2 min, followed by 94 °C for 30 s, 60 °C for 30 s, 72 °C for 30 s for 40 cycles, and a final extension at 68 °C for 7 min. The PCR product was cloned into the mammalian expression vector pcDNA3.1™D/V5-His-TOPO® (Invitrogen) using the pcDNA3.1™ Directional TOPO® expression kit (Invitrogen), according to the manufacturer's protocol. The *KLK14* sequence within the construct, denoted pcDNA3.1-*KLK14*, was confirmed with an automated DNA sequencer using vector-specific primers in both directions.

Human embryonic kidney (HEK)-293 cells (American Type Culture Collection (ATCC), Manassas, VA) were stably transfected with 3 μg of PmeI-linearized pcDNA3.1-*KLK14* by lipofection using PolyFect transfection reagent (Qiagen, Valencia, CA), according to the manufacturer's instructions. Transfected HEK-293 cells were incubated in Dulbecco's modified Eagle's medium (DMEM; Invitrogen) supplemented with 10% fetal bovine serum (FBS), in a humidified atmosphere containing 5% CO_2. After 48 h, cells were re-plated into 35-mm dishes, and the selection agent Geneticin (G418, 300 μg/ml final concentration; Invitrogen) was added. Resistant clones were chosen over 14 days under continuous G418 selection and cultured separately in 24 wells followed by 6-well plates. One clone, denoted P1–4, was selected for large scale expression of pro-KLK14 and grown in DMEM with 10% FBS until 80% confluency. At this stage, the media were replaced with serum-free CD Chinese hamster ovary media supplemented with GlutaMax™I (8 mM final concentration; Invitrogen). Conditioned media was collected by centrifugation after 10 days of incubation.

Recombinant pro-KLK14 was purified to homogeneity from the conditioned serum-free media of HEK-293 cells stably transfected with pcDNA3.1-*KLK14* sequentially by cation-exchange and reversed-phase chromatography. Prior to purification, 1 liter of media was prepared as described above for yeast culture supernatant. Concentrated CM was diluted 1:4 in 10 mM MES (pH 5.3) and applied to a previously equilibrated 5-ml SP HP-Sepharose column (GE Healthcare), previously equilibrated with 10 mM MES (pH 5.3), on the ÁKTA fast performance liquid chromatography system at a flow rate of 1 ml/min. Pro-KLK14 was eluted with a multistep salt gradient of 1 M KCl in 10 mM MES (pH 5.3) at a flow rate of 3 ml/min as follows: (*a*) continuous linear gradient of 0–0.25 M KCl for 17 min, (*b*) maintenance at 0.25 M KCl for 33 min, (*c*) linear gradient of 0.25–0.35 M KCl for 8.3 min, (*d*) maintenance at 0.35 M KCl for 33 min, and (*e*) followed by a linear gradient of 0.35-0.8 M KCl for 33 min. Elution fractions (3 ml) were analyzed by our newly developed enzyme-linked immunosorbent assay (ELISA; described herein) and by detection methods mentioned below. Fractions containing pro-KLK14 were then pooled, concentrated, and supplemented with a final concentration of 1% trifluoroacetic acid and loaded in 0.1% trifluoroacetic acid in H_2O onto a 1-ml Vydac C4 reversed-phase column (The Separations Group, Inc., Hesperia, CA) connected to an Agilent series 1100 HPLC system equipped with a diode array detector (Agilent Technologies, Inc, Palo Alto, CA). Elution was performed with a multistep acetonitrile (ACN) gradient at a flow rate of 0.8 ml/min consisting of 5-min linear gradients of 20–25, 25–30, 30–32, 32–35, 35–40, and 40–100% ACN intervened by 15-min steps at 25, 30, 32, and 35% ACN. ACN was removed from each fraction by evaporation with nitrogen gas at a pressure of 15 p.s.i.

For both recombinant KLK14 proteins, purity was assessed on silver-stained SDS-polyacrylamide gels (described below). Concentration was determined by the BCA method (Pierce), and protein identity was confirmed by tandem mass spectrometry, as described previously (23). Proteins were aliquoted and stored at −80 °C in 0.1 M sodium acetate buffer (pH 5.0).

Detection of Recombinant KLK14

To monitor recombinant KLK14 production, purification, and/or activity, samples were analyzed by SDS-PAGE, Western blot, and zymography.

SDS-PAGE—SDS-PAGE was performed using the NuPAGE BisTris electrophoresis system and precast 4–12% gradient polyacrylamide gels at 200 V for 30 min (Invitrogen). Proteins were visualized with a Coomassie G-250 staining solution, SimplyBlue™ SafeStain (Invitrogen), and/or by silver staining with the Silver Xpress™ kit (Invitrogen), according to the manufacturer's instructions.

Western Blots—For immunodetection of KLK14, proteins resolved by SDS-PAGE were subsequently transferred onto a Hybond-C Extra nitrocellulose membrane (GE Healthcare) at 30 V for 1 h. The membrane was blocked with Tris-buffered saline/Tween (0.1 mol/liter Tris-HCl buffer (pH 7.5) containing 0.15 mol/liter NaCl and 0.1% Tween 20) supplemented with 5% nonfat dry milk overnight at 4 °C and probed with a KLK14 polyclonal rabbit antibody (produced in-house; diluted 1:2000 in Tris-buffered saline/Tween) for 1 h at room temperature. The membrane was washed three times for 15 min with Tris-buffered saline/Tween and treated with alkaline phosphatase-conjugated goat anti-rabbit antibody (1:10,000 in Tris-buffered saline/Tween; Jackson ImmunoResearch) for 1 h at room temperature. Finally, the membranes were washed again as above, and fluorescence was detected on x-ray film using chemiluminescent substrate (Diagnostic Products Corp., Los Angeles).

Zymography—The proteolytic activity of recombinant KLK14 proteins was visualized by gelatin zymography (Invitrogen). Recombinant KLK14 was diluted 1:1 in Tris-glycine SDS sample buffer and electrophoresed on precast Novex® 10% gelatin zymogram gels (Invitrogen) at 125 V for 2.5 h at 4 °C. The gels were subsequently incubated in zymogram renaturing buffer (Invitrogen) for two 30-min intervals at room temperature, followed by incubation in zymogram developing buffer (Invitrogen) for 3 h at 37 °C. Gels were stained with SimplyBlue™ SafeStain and destained until the white lytic bands corresponding to areas of protease activity were visible.

Generation of Antibodies against KLK14

New Zealand White female rabbits and BALB/c female mice were repeatedly immunized with purified recombinant mature KLK14 (100 μg) for polyclonal and monoclonal antibody development, respectively. KLK14 was diluted 1:1 in complete Freund's adjuvant for the first injection and in incomplete Freund's adjuvant for subsequent injections. Injections were repeated three times for mice and six times for rabbits at 3-week intervals. The polyclonal sera were tested every 2 weeks by an immunofluorometric method described in detail elsewhere (10), until the highest antibody titers against KLK14 were detected.

Monoclonal antibodies against KLK14 were produced by standard hybridoma technology. The splenocytes from preselected immunized mice were fused with the Sp2/0 myeloma cells using polyethylene glycol 1500. The resultant hybridoma cells were cultured in 96-well plates in DMEM (Invitrogen) containing 20% FBS, 200 mM glutamine, 1% OPI (oxaloacetic

acid, pyruvic acid, insulin), and 2% HAT (hypoxanthine, aminopterin, thymidine; Sigma) for selection at 37 °C, 5% CO_2 for 10–14 days. Hybridoma supernatants were collected and screened by an immunofluorometric technique described previously (24). Positive clones were then expanded sequentially in 24- and 6-well plates in complete media (reducing the FBS to 15% and changing the HAT to HT). Antibody isotyping was subsequently performed using a mouse immunoglobulin subtype identification kit (Sigma) to isolate clones producing anti-KLK14 monoclonal antibodies of the IgG class. One positive hybridoma clone, denoted 2E9, was expanded in flasks in serum-free CD Chinese hamster ovary media (Invitrogen) containing 200 mM glutamine, for large scale antibody production. Anti-KLK14 monoclonal antibody 2E9 was purified from the culture supernatant using the Affi-Gel Protein-A MAPS II kit (Bio-Rad), according to manufacturer's instructions, and used in subsequent immunoassay development.

Development of an ELISA for KLK14

A "sandwich-type" ELISA, with a mouse monoclonal/rabbit polyclonal configuration, was developed as follows. The KLK14-specific monoclonal antibody (clone 2E9; developed in-house) was first immobilized on a 96-well white polystyrene plate (500 ng/well) by incubating in coating buffer (50 mmol/liter Tris, 0.05% sodium azide (pH 7.8)) overnight at room temperature. The plate was then washed three times with washing buffer (50 mmol/liter Tris, 150 mmol/liter NaCl, 0.05% Tween 20 (pH 7.8)). KLK14 standards or samples were then pipetted into each well (100 μl/well, diluted 1:1 in assay buffer (50 mmol/liter Tris, 6% bovine serum albumin, 10% goat IgG, 2% mouse IgG, 1% bovine IgG, 0.5 mol/liter KCl, 0.05% sodium azide (pH 7.8)), incubated for 2 h with shaking, and then washed six times, as above. Subsequently, 100 μl of rabbit anti-KLK14 polyclonal sera (developed in-house) diluted 1000-fold in assay buffer was added and incubated for 1 h. After incubation, the plate was washed as above, and alkaline phosphatase-conjugated goat anti-rabbit IgG (Jackson ImmunoResearch), diluted 3000-fold in assay buffer, was applied and plates were incubated for 45 min. After washing as above, the alkaline phosphatase substrate diflunisal phosphate (100 μl of a 1 mM solution) in substrate buffer (0.1 mol/liter Tris (pH 9.1), 0.1 mol/liter NaCl, and 1 mmol/liter $MgCl_2$) was added to each well and incubated for 10 min followed by addition of developing solution (100 μl, containing 1 mol/liter Tris base, 0.4 mol/liter NaOH, 2 mmol/liter $TbCl_3$, and 3 mmol/liter EDTA) for 1 min. The resultant fluorescence was measured by time-resolved fluorometry on the Cyberfluor 615 Immunoanalyzer (MDS Nordion, Kanata, Ontario, Canada). Calibration and data reduction were performed automatically, as described elsewhere (25).

The optimal assay configuration and conditions described above were obtained by testing several monoclonal antibody and polyclonal sera dilutions and diluents, as well as different incubation times for each step of the procedure. Assay sensitivity (detection limit), specificity (including cross-reactivity to other KLK family members), linearity, recovery, and within-run and between-run imprecisions were determined as described previously (10).

Tissue Extracts, Biological Fluids, and Cancer Cell Lines

The concentration of KLK14 in normal and cancerous tissue extracts, biological fluids, and conditioned media of various cancer cell lines was determined with the newly developed KLK14-specific ELISA.

Tissue Extracts—A panel of 40 normal tissue extracts were prepared as described elsewhere (10), including adrenal gland, axillary lymph node, bone, breast, colon, endometrium, esophagus, fallopian tube, kidney, liver, lung, mesenteric lymph node, skeletal muscle, ovary, pancreas, prostate, seminal vesicle, skin, small intestine, spleen, stomach, testis, thyroid, trachea, ureter, uterus, salivary gland, pharyngeal tonsil, placenta, cervix, cerebellum, frontal lobe cortex, hippocampus, medulla, midbrain, occipital cortex, pituitary, pons, temporal lobe cortex, and spinal cord. Cancerous ovarian tissues, containing >80% tumor cells, were obtained from patients with primary epithelial ovarian cancer who underwent surgery and treatment for ovarian cancer at the Department of Gynecology of the University of Turin, Turin, Italy, between July of 1991 and April of 1999. Ovarian tumor cytosolic extracts were prepared as described previously (26). Total protein content of the extracts was determined using the bicinchoninic acid method, with bovine serum albumin as a standard (Pierce).

Biological Fluids—Cerebrospinal fluid, breast milk, amniotic fluid, seminal plasma, ascites fluid from ovarian cancer patients, breast cancer cytosolic extracts, and sera from males and females without known disease and of prostate cancer patients were residual samples submitted previously for routine biochemical testing and stored at −80 °C. Investigations were carried out in accordance with the ethical standards of the Helsinki Declaration of 1975, as revised in 1983, and have been approved by the Institutional Review Board of Mount Sinai Hospital, Toronto, Canada, and the Institute of Obstetrics and Gynecology, Turin, Italy.

Cell Lines—The astrocytoma cell line, SW-1088 (HTB12); breast cancer cell lines MDA-MB-468 (HTB132), BT-474 (HTB-20), T-47D (HTB-133), MCF7 (HTB-22), and ZR-75, MFM223, MDA-MB-231 (HTB-26), MDA-MB-453 (HTB-131), MDA-MB-361 (HTB27), BT-20 (HTB19); the colorectal adenocarcinoma cell line, COLO 320HSR (CCL-220.1); the ovarian cancer cell lines Caov-3 (HTB-75), MDAH 2774 (CRL-10303), TOV-21G (CRL-11730), TOV112D (CRL-11731), OVCAR-3 (HTB-161), OV-90 (CRL-11732), ES2 (CRL-1978); the cervical cancer cell lines HeLa (CCL-2), C-4 I (CRL-1594), ME-180 (HTB-33), HT-3 (HTB-32); neuroblastoma cell lines SK-N-DZ (CRL-2149) and IMR-32 (CCL-127) and neuroepithelioma cell line Sk-N-MC (HTB-10); the pancreatic cancer cell line, MIA PaCa-2 (CRL-1420); and the prostate cancer cell line LNCaP (CRL-1740) were purchased from ATCC. The BG-1 ovarian cancer cell line was kindly provided by Dr. Henri Rochefort (Montpellier University, Montpellier, France), and the PC-3 cell line, stably transfected with androgen receptor (PC-3 $(AR)_6$); was provided by Dr. Theodore Brown (Samuel Lunenfeld Research Institute, Mount Sinai Hospital, Toronto, Canada). Cells were cultured to near confluency in RPMI medium (Invitrogen) supplemented with glutamine (200 nM) and FBS (100 ml/liter) in plastic flasks.

Protease Assays and Kinetic Constant Determinations

7-Amino-4-methylcoumarin (AMC) was purchased from Sigma. The following synthetic AMC substrates were obtained from Bachem Bioscience (King of Prussia, PA): Boc-Phe-Ser-Arg-AMC (FSR-AMC), Boc-Val-Pro-Arg-AMC (VPR-AMC), H-Pro-Phe-Arg-AMC (PFR-AMC), benzyloxycarbonyl-Gly-Gly-Arg-AMC (GGR-AMC), Boc-Leu-Gly-Arg-AMC (LGR-AMC), Boc-Leu-Lys-Arg-AMC (LKR-AMC), Boc-Leu-Arg-Arg-AMC (LRR-AMC), Boc-Gln-Arg-Arg-AMC (QRR-AMC), Boc-Gln-Ala-Arg-AMC (QAR-AMC), Boc-Gln-Gly-Arg-AMC (QGR-AMC), Tos-Gly-Pro-Arg-AMC (GPR-AMC), Tos-Gly-Pro-Lys-AMC (GPK-AMC), Boc-Glu-Lys-Lys-AMC (EKK-AMC), Boc-Val-Leu-Lys-AMC (VLK-AMC), and Suc-Ala-Ala-Pro-Phe-AMC (AAPF-AMC). Suc-Leu-Leu-Val-Tyr-AMC (LLVY-AMC) was purchased from the Peptide Institute Inc. (Osaka, Japan). All substrates were diluted in dimethyl sulfoxide (Me_2SO) to a final concentration of 80 mM and stored at −20 °C.

Individual AMC-peptide substrates (final concentrations ranging from 0.004 to 2 mM) were incubated with recombinant mature KLK14 (final concentration of 12 nM) at a final volume of 100 μl under optimal buffer conditions within 96-well white polystyrene microtiter plates. Reaction mixtures contained less than 5% (v/v) Me_2SO. Initial rates of KLK14-mediated peptide hydrolysis was monitored by measuring free AMC fluorescence on the Wallac 1420 Victor^{2TM} fluorometer (PerkinElmer Life Sciences) with excitation and emission filters set at 380 and 480 nm, respectively, at 1-min intervals for 20 min at 37 °C. KLK14-free reactions, for each peptide concentration, were used as negative controls, and background counts obtained were subtracted from each value. A standard curve was constructed using known concentrations of AMC in order to calculate the rate of free AMC release. The slope of the resultant AMC standard curve was 19.184 AMC fluorescence counts/nM free AMC. The steady-state (Michaelis-Menten) kinetic constants (k_{cat}/K_m) were then calculated by nonlinear regression analysis using Enzyme Kinetics Module 1.1 (Sigma Plot). All experiments were performed in triplicate and repeated at least twice.

Pro-KLK14 Activation Studies

The possible activation of pro-KLK14 by recombinant mature KLK5 (produced in-house in *P. pastoris* as described previously (27)) was monitored via complex formation between KLK14 and the serine protease inhibitor (serpin) α_1-antitrypsin (AT), an inhibitor of KLK14, but not of KLK5 (27). Pro-KLK14 was preincubated with KLK5 in a final volume of 10 μl at different molar ratios and incubation times. AT was then added at a 2-fold molar excess to a final volume of 15 μl. The reaction was incubated for 30 min at room temperature. As controls, AT was incubated alone and with recombinant mature KLK14 and pro-KLK14 and with mature KLK5. Reaction mixtures were resolved by SDS-PAGE under reducing conditions, and resultant gels were silver-stained.

Inhibition Assays, Serpins—Serine protease inhibitors (serpins), AT (SERPINA1), α_1-antichymotrypsin (ACT; SERPINA3), antithrombin III (ATIII; SERPINC1), α_2-antiplasmin (AP; SERPINF2), and plasminogen activator inhibitor-1 (PAI-1; SERPINE1) were purchased from Calbiochem. Inhibitors displayed >95% purity on Coomassie Blue-stained polyacrylamide gels, were diluted in water to a final concentration of 1 mg/ml, and were stored at −20 °C. To calculate second-rate constants, the inhibition of KLK14 by serpins was performed under pseudo-first order conditions, as described previously (28–30). KLK14 was preincubated with each serpin for various lengths of time (0–5 min for AT, AP, and PAI-1; 0–10 min for ATIII, and 0–60 min for ACT) and at different KLK14:serpin molar ratios at room temperature (for AT, AP, PAI-1 and ATIII) or 37 °C (for ACT) with gentle agitation. The reaction was quenched by diluting 10 μl in 190 μl of optimal buffer containing 0.2 mM QAR-AMC. AMC fluorescence was measured on the Wallac 1420 Victor^{2TM} fluorometer, as described above. All experiments were performed in triplicate.

To monitor KLK14-serpin complex formation, KLK14 (0.5 μg; 1 μM final concentration) was incubated with each serpin at molar ratios of 1:1, 1:2, 1:5, and 1:10 at room temperature for 30 min (for AT, AP, PAI-1 and ATIII) or at 37 °C for 1 h (for ACT). Reaction mixtures were resolved by SDS-PAGE under reducing conditions; gels were stained with SimplyBlue^{TM} SafeStain.

Effect of Ions on KLK14 Activity

KLK14 was incubated with each cation and citrate (solutions prepared from salts of $ZnCl_2$, $ZnSO_4$, $Zn(CH_3COO)_2$, $CaCl_2$, $MgCl_2$, NaCl, KCl, sodium citrate, at final concentrations of 0, 12, 60, 120, 1200, and 12,000 nM) in optimal assay buffer at a final volume of 100 μl for 10 min at 37 °C with gentle agitation. At this point, QAR-AMC (at a final concentration of 0.5 mM) was applied to each reaction mixture, and AMC fluorescence was measured on the Wallac 1420 Victor^{2TM} fluorometer, as described above. Residual KLK14 activity against QAR-AMC after incubation with individual cations/citrate was calculated.

Reversal of Zn^{2+} Inhibition of KLK14 by EDTA

KLK14 (12 nM final concentration) was incubated alone or with the following: (*a*) Zn^{2+} (1.2 μM final concentration $ZnCl_2$), (*b*) EDTA (1 mM final concentration), (*c*) Zn^{2+} and EDTA, and (*d*) Zn^{2+} followed by the addition of EDTA after 20 min, at a final volume of 100 μl in optimal assay buffer in microtiter plate wells for 10 min at 37 °C with gentle agitation. After incubation, QAR-AMC (final concentration of 0.5 mM) was applied to each well. AMC fluorescence was measured on the Wallac 1420 Victor^{2TM} fluorometer, as described above. KLK14-free reactions were used as negative controls, and background fluorescence was subtracted from each value. All experiments were performed in triplicate.

In Vitro Proteolysis Experiments

The following substrates were incubated with KLK14: mouse sarcoma collagen type I, chicken sternal cartilage collagen type II, calf skin collagen type III, human placenta collagen type IV, human foreskin fibroblast fibronectin, human plasma vitronectin, laminin, and low molecular weight kininogen were purchased from Sigma. Plasminogen from human plasma and recombinant human insulin-like growth factor-binding proteins 2 and 3 (IGFBP-2 and IGPBP-3) were obtained from R&D Systems Inc. (Minneapolis, MN).

Collagen I, II, and III (2 μg); collagen IV, laminin, fibronectin, kininogen (5 μg); fibrinogen, plasminogen (10 μg); and vitronec-

tin, IGFBP-2, and IGFBP-3 (300 ng) were incubated with specific amounts of KLK14 (6 ng to 1 μg) in optimal assay buffer over time at room temperature or 37 °C with gentle agitation. KLK14-free reactions were included as negative controls. Reactions were terminated by freezing in liquid nitrogen and resolved by reducing SDS-PAGE, as described above. Gels were stained with SimplyBlue™ SafeStain or with the Silver Xpress™ kit (Invitrogen).

Furthermore, KLK14 (0.4 and 0.8 μg) was incubated with fluorescent conjugates of collagen types I and IV (2.5 μg) and fibrinogen (3.75 μg) (Molecular Probes, Eugene, OR) in optimal assay buffer (final volume 200 μl) at room temperature. Fluorescence was measured every 10 min for 2 h on the Wallac 1420 Victor^{2TM} fluorometer set at 492 nm for excitation and 535 nm for emission. Enzyme-free reactions were used as negative controls, and background fluorescence was subtracted from each value. All experiments were performed in triplicate.

N-terminal Sequencing

N-terminal sequence analysis was performed on KLK14-generated fragments derived from recombinant mature KLK14, fibronectin, collagen IV, plasminogen, kininogen, fibrinogen, and vitronectin. KLK14 was incubated alone (3 μg) or with each intact protein (2.5–5 μg) for different time points as specified by the proteolysis experiments, separated by reducing SDS-PAGE, and transferred to a polyvinylidene difluoride membrane (GE Healthcare), previously immersed in 100% methanol at 30 V for 1 h. After the transfer, the membrane was removed and rinsed with de-ionized water, stained with Coomassie Blue R-250 (0.1% solution in 40% methanol) for 5 min, and de-stained for 5 min in 50% methanol. The membrane was then thoroughly washed with de-ionized water and air-dried. Fragments were excised and subjected to automated N-terminal Edman degradation (31) consisting of five cycles of Edman chemistry on a 492 Procise cLC sequencer (Applied Biosystems, Foster City, CA), followed by analysis of resultant phenylthiohydantoin-derivative residues on an HPLC column.

RESULTS

Recombinant Mature and Pro-KLK14

Recombinant mature and pro-KLK14 proteins were produced in their native forms, without fusion tags, in yeast (*P. pastoris*) and mammalian (HEK-293) expression systems, respectively. Secreted expression was achieved by cloning *KLK14* cDNA in-frame with the yeast α-factor for mature KLK14 and with the native KLK14 signal sequence in the case of pro-KLK14. As monitored by SDS-PAGE, Western blot analysis and/or ELISA, mature KLK14 was detected in the yeast culture supernatant after 1 day of methanol induction, with the highest levels produced after 6 days; maximal pro-KLK14 levels were attained after a 10-day incubation period in serum-free media (data not shown). After their respective two-step chromatographic purification procedures, recombinant mature and pro-KLK14 were obtained with >95% purity, as verified by silver-stained polyacrylamide gels (Fig. 1*A*). The yield of purified mature and pro-KLK14 from 1-liter culture supernatants was in the range of 1.5–3 mg and 25–50 μg, respectively, as determined by ELISA and total protein assays.

Prepro-KLK14 is a 251-amino acid polypeptide consisting of a signal sequence (Met^{1}–Ser^{18}), followed by a 6-amino acid pro-peptide (Gln^{19}–Lys^{24}) and a 227-amino acid trypsin-like serine protease domain (Ile^{25}–Lys^{251}) with a predicted zymogen activation site at Lys^{24}–Ile^{25} (7, 8). The resultant masses of both recombinant proteins were consistent with those inferred from the primary KLK14 sequence, indicating a lack of glycosylation or other post-translational modifications. Purified mature KLK14 appeared as an enzymatically active intact band of ~25 kDa along with 8 less abundant lower molecular weight bands, identified as products of autodegradation (Fig. 1, *lane 1*, and Fig. 4). Purified pro-KLK14 was visualized as a single, enzymatically inactive band of ~27 kDa, as expected (Fig. 1, *lane 2*).

The identity of both recombinant KLK14 proteins was verified by Western blotting (Fig. 1*B*) and confirmed by tandem

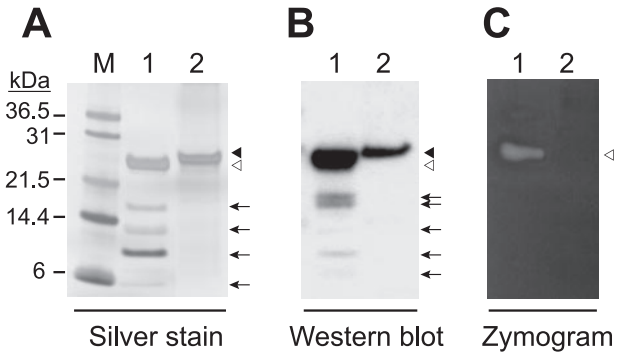

FIGURE 1. **Purified recombinant mature and pro-KLK14.** *A–C, lane 1*, mature KLK14; *lane 2*, pro-KLK14. *A*, silver-stained reducing SDS-PAGE of KLK14 (300 ng/lane). *B*, immunodetection of KLK14 using a primary rabbit polyclonal antibody (1:2000) generated against mature KLK14. *C*, gelatin zymography of KLK14. Intact mature KLK14 is represented by a single band of 25 kDa (△); lower molecular weight bands likely correspond to autodegradation products and are indicated with *arrows* (←). Pro-KLK14 is visualized as a single band of 27 kDa (▲). Zymographic analysis reveals that only mature KLK14 is active, as expected. *M*, molecular mass standards in kDa.

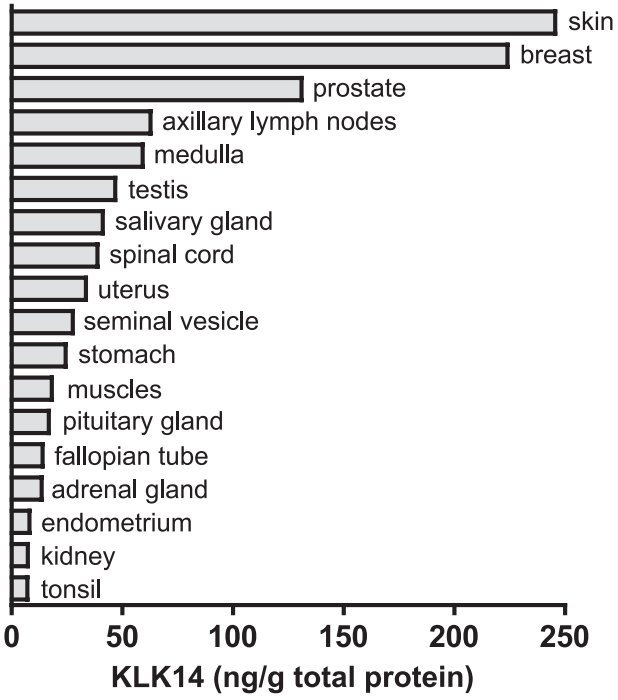

FIGURE 2. **Concentration of KLK14 in adult human tissue extracts.** The amount of KLK14 in tissue extracts is corrected for the total protein content and is expressed as nanograms of KLK14 per g of total protein.

TABLE 1
Summary of KLK14 levels in various biological fluids

Biological fluid	No. of samples tested	KLK14 concentration (μg/liter)			Positivity
		Range	Mean (S.D.)	Median	
					%
Seminal plasma	24	3.6–82.5	15.8 (16.0)	13.0	100
Amniotic fluid	24	1.7–22.9	8.1 (6.0)	6.0	100
Saliva	6	0.6–6.1	4.4 (2.1)	5.3	100
Follicular fluid	19	0–8.8	1.27 (2.13)	0.44	95
Breast milk	18	0–18.6	1.2 (0.42)	0.13	83
Serum					
Female	32	0.03–0.25	0.14 (0.05)	0.14	100
Male	17	0.04–0.24	0.12 (0.05)	0.10	100
Cerebrospinal fluid	6	0	0	0	0

mass spectrometry. In the case of recombinant KLK14, partially sequenced tryptic peptides IITGGHTCT, QVTHPNYNSR, and QACASPGTSCR corresponded to amino acid sequences 25–33, 97–106 and 134–144, respectively, of the KLK14 protein sequence. Likewise, sequenced peptide fragments obtained from the pro-KLK14 sample included IIGGHTCTR, SSQPWQAALLAGPR, QVTHPNYNSR, AVRPIEVTQACASPGTSCR, and DSCQGDSGGPLVCR, which matched precisely with KLK14 amino acid sequences 25–33, 34–47, 97–106, 126–144, 198–211, respectively (numbering is based on GenBank™ accession number AAK48524).

Distribution of KLK14 in Tissues, Fluids, and Cell Lines

A novel KLK14-specific ELISA was established to quantify KLK14 levels in normal and cancerous tissue extracts, biological fluids, and cell lines. The optimized KLK14-ELISA, consisting of monoclonal antibody 2E9 (capture antibody) and polyclonal rabbit antiserum (detection antibody) generated against recombinant mature KLK14, is sensitive (detection limit of 0.05 μg/liter), specific for KLK14 (<0.1% cross-reactivity with other KLKs), recognizes both mature and pro-KLK14 recombinant proteins, and is linear from 0.05 to 10 μg/liter with between-run and within-run coefficients of variation of <10%.

Among the 40 normal adult human tissues screened for KLK14 content, 18 contained detectable levels of KLK14 (Fig. 2). The highest KLK14 levels were found in skin (245 ng/g total protein), followed by breast (224 ng/g total protein) and prostatic (131 ng/g total protein) tissue extracts, in general accord with previous studies (7;8;10;11;13–15;17). Comparatively lower levels were observed in axillary lymph nodes (62.8 ng/g total protein) and medulla (59.2 ng/g total protein) extracts with minor amounts (<50 ng/g total protein) in the remaining tissues.

The concentration of KLK14 in biological fluids from healthy individuals was quantified (Table 1). In agreement with our prior study (10), the highest levels of KLK14 were measured in seminal plasma (15.8 ± 16.0 μg/liter), followed by amniotic fluid (8.1 ± 6.0 μg/liter) and saliva (4.4 ± 2.1 μg/liter). Follicular fluid and breast milk contained lower concentrations (~1.2 μg/liter). KLK14 was not detected in the cerebrospinal fluid samples examined. Compared with normal, KLK14 levels were elevated in the serum of patients with prostate cancer (Fig. 3), a likely consequence of *KLK14* overexpression and secretion by prostate tumor tissues (17). We also detected KLK14 in ascites fluids from ovarian cancer patients (0.34 ± 0.7 μg/liter) as well as in cytosolic extracts of ovarian (1.77 ± 5.13 μg/liter) and breast (0.26 ± 1.17 μg/liter) tumors.

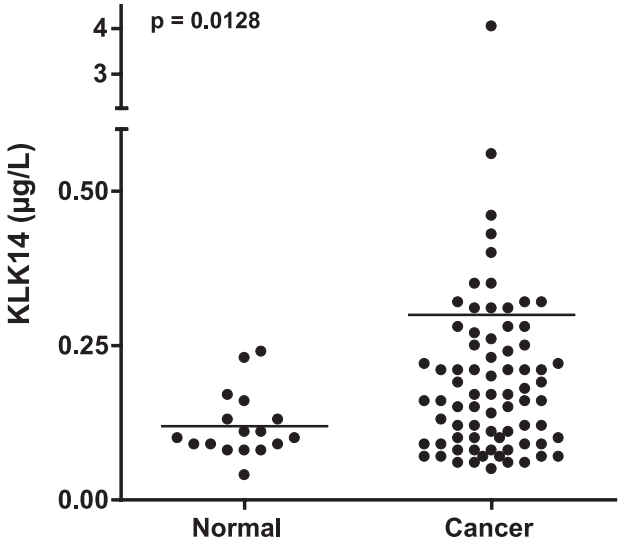

FIGURE 3. **Elevation of KLK14 in serum of prostate cancer patients.** Distribution of KLK14 levels (μg/liter) in the sera of healthy males (normal) and patients with prostate cancer. The *p* value was determined by the Mann-Whitney *U* test. *Horizontal lines* represent the median values.

Among the cell lines studied, KLK14 was only detected in the conditioned media of a nontumorigenic keratinocyte cell line (HaCaT; 0.275 μg/liter) and a subset of neuroblastoma (Sk-N-MC, IMR32; 0.949 and 0.193 μg/liter, respectively), breast cancer (MCF7, MDA-MB-468; 0.116 and 0.497 μg/liter, respectively), cervical cancer (C-4 I, ME-180, HT-3; 0.158–0.456 μg/liter), and ovarian cancer (TOV-21G, MDAH 2774, OV-90, TOV112D; 0.103–0.604 μg/liter) cell lines.

Autodegradation of KLK14 in Vitro

Purified recombinant mature KLK14 consisted of a mixture of peptides visualized as multiple bands under reducing SDS-PAGE (Fig. 4*A*). Western blot (Fig. 1*B*) and N-terminal sequence analysis confirmed the identity of the low molecular weight (<25 kDa) protein bands as internal fragments of mature KLK14 likely arising from auto-proteolytic cleavage (Fig. 4). All KLK14 cleavage sites occurred after P1-Arg residues (Fig. 4*B*), and the majority reside in exposed, solvent-accessible surface loops, which are most susceptible to proteolytic cleavage (Fig. 4*C*). Among KLK14 autodegradation fragments, only fragment I retains all residues of the catalytic triad (His^{67}, Asp^{111}, and Ser^{204}; see Fig. 4*B*) and may exhibit residual serine protease activity. However, prolonged incubation (24 h) of mature KLK14 at 37 °C resulted in complete hydrolysis of the

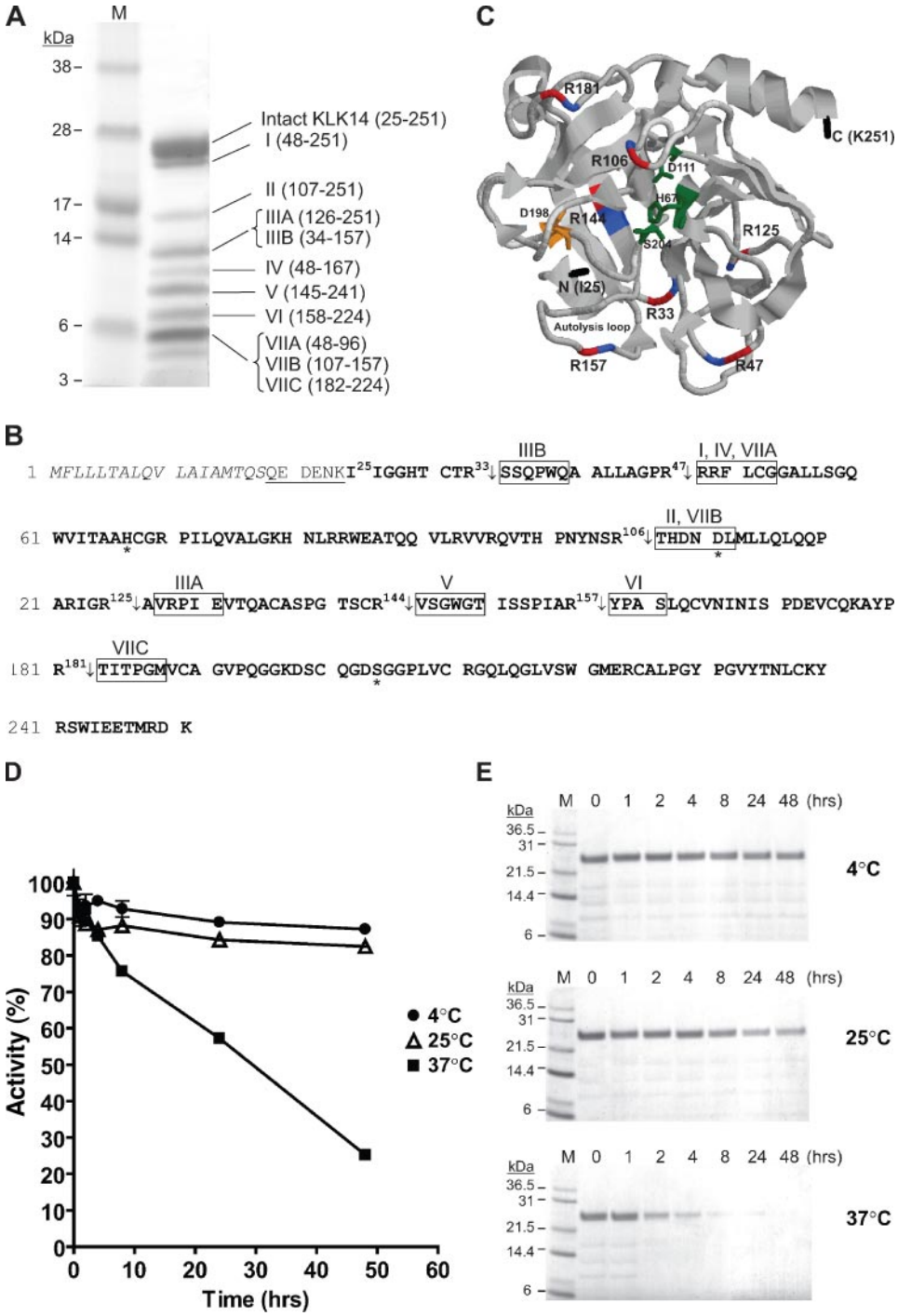

FIGURE 4. **Autodegradation of KLK14.** *A,* Coomassie Blue-stained SDS-polyacrylamide gel of fragmented mature recombinant KLK14 (5 μg). Intact KLK14 corresponds to the 25-kDa band. Lower molecular weight autodegradation fragments of KLK14 are labeled *I–VII*. The region that each peptide fragment spans within the KLK14 protein sequence is in *parentheses.* Note that protein bands III and VII are comprised of 2 and 3 individual peptides, respectively. *M*, molecular mass standards in kDa. *B,* location of the N-terminal sequence of each KLK14 degradation fragment within the primary KLK14 protein sequence. Prepro-KLK14 is formed of a signal peptide (*italics*), followed by a pro-peptide (*underlined*) and the mature sequence containing the serine protease domain (*boldface*). Catalytic triad (His^{67}, Asp^{111}, and Ser^{204}) residues are indicated with an *asterisk*. The N-terminal sequence of KLK14 degradation fragments is *boxed*, with the corresponding label above. Cleavage sites are indicated by an *arrow*; the P1 amino acid is numbered. *A* and *B*, KLK14 sequences are numbered from the N terminus of prepro-KLK14 based on GenBank™ accession number AAK48524. *C,* location of autolytic cleavage sites within the theoretical tertiary structure of mature KLK14, as predicted by homology modeling. The ribbon plot of mature KLK14 is shown in the traditional serine protease standard orientation (*i.e.* looking into the active site cleft) (86). Secondary structure elements are displayed as *arrows* (β-strands) and *ribbons* (α-helices). The position of the autolysis loop is indicated. N- and C-terminal residues are shown in *black*; the side chains of the catalytic triad residues are shown in *green*; S1 side chain is colored *orange.* KLK14 cleavage sites, *i.e.* P1 and P1′ residues, are shown in *red* and *blue*, respectively, and P1-R residues are labeled. *D,* inactivation of KLK14 by autodegradation. KLK14 was incubated alone at 4 °C (●), 25 °C (△), and 37 °C (■) over time (0–48 h). *E,* SDS-PAGE analysis of KLK14 autodegradation over time at 4, 25, and 37 °C. Time points are indicated *above* each lane. *M*, molecular mass standards in kDa.

intact 25-kDa band and a corresponding decrease in enzymatic activity (Fig. 4, *D* and *E*). Auto-inactivation of KLK14 by autolytic cleavage may represent a potential regulatory mechanism.

Optimal pH and Buffer Composition for KLK14 Activity

Two buffer systems, 100 mM Na_2HPO_4 (pH 7–10) and 100 mM Tris-HCl (pH 6–9), were chosen to determine the optimal pH for KLK14 activity. Although KLK14 was most active at a pH of 8.0 in both systems, KLK14 activity was 1.4-fold higher in phosphate *versus* Tris buffer. Furthermore, KLK14 displayed enhanced activity (13% increase) in the presence of 0.01% Tween 20 compared with 0.2% bovine serum albumin in which activity decreased 30% (Tween 20 and bovine serum albumin prevent adsorption of KLK14). Hence, the buffer composition utilized in subsequent studies was 100 mM Na_2HPO_4, 0.01% Tween 20 (pH 8.0).

Activation of Pro-KLK14

As with other S1A family SP, pro-KLK14 requires the removal of the inhibitory N-terminal pro-peptide sequence at Lys^{24}–Ile^{25} for conversion into its enzymatically active form. Autoactivation is not expected to occur because P1-Lys residues are unfavored by KLK14 (21) (see below). Indeed, purified recombinant pro-KLK14 remained as an enzymatically inactive, intact ~27-kDa band on SDS-PAGE and zymographic analyses after prolonged incubation (data not shown), which is supported by previous findings (19).

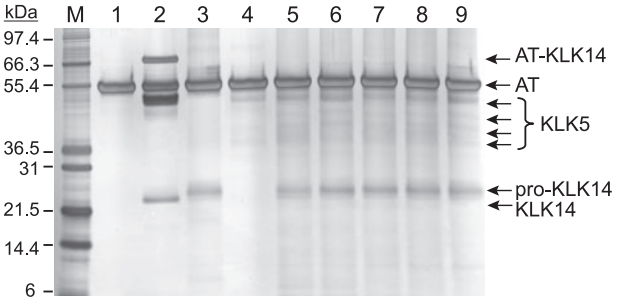

FIGURE 5. **Lack of pro-KLK14 activation by KLK5.** Pro-KLK14 (0.5 μM) was incubated with KLK5 (0.1 μM) for 0, 10, and 30 min and 1 and 3 h at 37 °C, after which AT, at a KLK14-AT molar ratio of 1:2, was added for 30 min at room temperature (*lanes 5–9*, respectively). Activation of pro-KLK14 was monitored by formation of the AT-KLK14 complex. As controls, AT was incubated alone (*lane 1*) and with mature KLK14 (*lane 2*), pro-KLK14 (*lane 3*), and mature KLK5 (*lane 4*). Note that an AT-KLK14 complex was not observed after incubation of pro-KLK14 with KLK5, indicating a lack of activation.

To test the potential activation of pro-KLK14 by KLK5, which is often co-expressed with KLK14 *in vivo* (32), we incubated pro-KLK14 with KLK5 and monitored the reaction via complex formation with AT. However, we were unable to provide evidence for the activation of pro-KLK14 by KLK5. Neither dose-dependent (data not shown) nor time-dependent activation of pro-KLK14 by KLK5 was observed in our study, as confirmed by the lack of KLK14-AT complex formation after incubation of pro-KLK14 with KLK5 (Fig. 5, *lanes 5–9*). As expected, mature KLK14 readily formed a complex with AT, whereas pro-KLK14 and KLK5 did not (Fig. 5, *lanes 2–4*). Our results are further substantiated by the fact that KLK5 is not able to cleave a heptapeptide encompassing the activation site of KLK14 (33) and that KLK5 generally favors Arg relative to Lys at P1 (27), *i.e.* the best P1-Arg containing substrate (VPR-AMC) was hydrolyzed at a 133-fold higher catalytic efficiency by KLK5 than the best P1-Lys containing substrate (VLK-AMC) (27). A prior study by Brattsand *et al.* (19) reported that KLK5 is an efficient activator of pro-KLK14. However, pro-KLK14 activation occurred after 24 h of incubation with KLK5, suggesting an inefficient conversion reaction, which may not be physiologically relevant. Furthermore, the reaction was monitored with a chromogenic substrate (Pro-Phe-Arg-*p*-nitroanilide) equally hydrolyzed by both KLK5 and KLK14. In our study, we utilized the serpin AT, an inhibitor that targets KLK14 but not KLK5 (27), to monitor pro-KLK14 activation over 3 h. Taken together, these results call into question the ability of KLK5 to efficiently activate pro-KLK14.

Substrate Specificity of KLK14

The substrate specificity of KLK14 was assessed by determining its relative hydrolytic activity and corresponding kinetic parameters (*i.e.* K_m and k_{cat}) against a panel of 16 synthetic substrates containing an AMC fluorogenic leaving group (Table 2). Among these AMC-peptides, 14 contain a basic P1 residue (Arg, Lys) and 2 contain bulky, hydrophobic amino acids at P1 (Tyr, Phe) and thereby represent substrates for

TABLE 2
Summary of steady-state parameters for hydrolysis of synthetic substrates by KLK14

Substrate	K_m	k_{cat}	k_{cat}/K_m	Activity
	mM	min^{-1}	$mM^{-1}\ min^{-1}$	%
Trypsin-like				
Boc-QAR-AMC	0.045 ± 0.0039	382.07	8516.94	100
Boc-VPR-AMC	0.043 ± 0.0067	361.08	8422.67	98.9
H-PFR-AMC	0.090 ± 0.018	137.49	1520.57	17.9
Boc-FSR-AMC	0.278 ± 0.027	388.68	1397.63	16.4
Boc-LGR-AMC	0.0577 ± 0.00680	78.12	1352.96	15.9
Boc-QGR-AMC	0.139 ± 0.0241	145.91	1051.98	12.4
Tos-GPR-AMC	0.173 ± 0.0187	139.01	803.53	9.4
Boc-QRR-AMC	0.0268 ± 0.00284	16.43	612.37	7.2
Benzlyoxycarbonyl-GGR-AMC	0.130 ± 0.0146	36.89	282.90	3.3
Boc-LKR-AMC	NR[a]			
Boc-LRR-AMC	NR[a]			
Boc-VLK-AMC	0.578 ± 0.0307	62.23	107.72	1.3
Tos-GPK-AMC	NR[a]			
Boc-EKK-AMC	NR[a]			
Chymotrypsin-like				
Suc-AAPF-AMC	NR[a]			
Suc-LLVY-AMC	NR[a]			

[a] NR indicates no reaction.

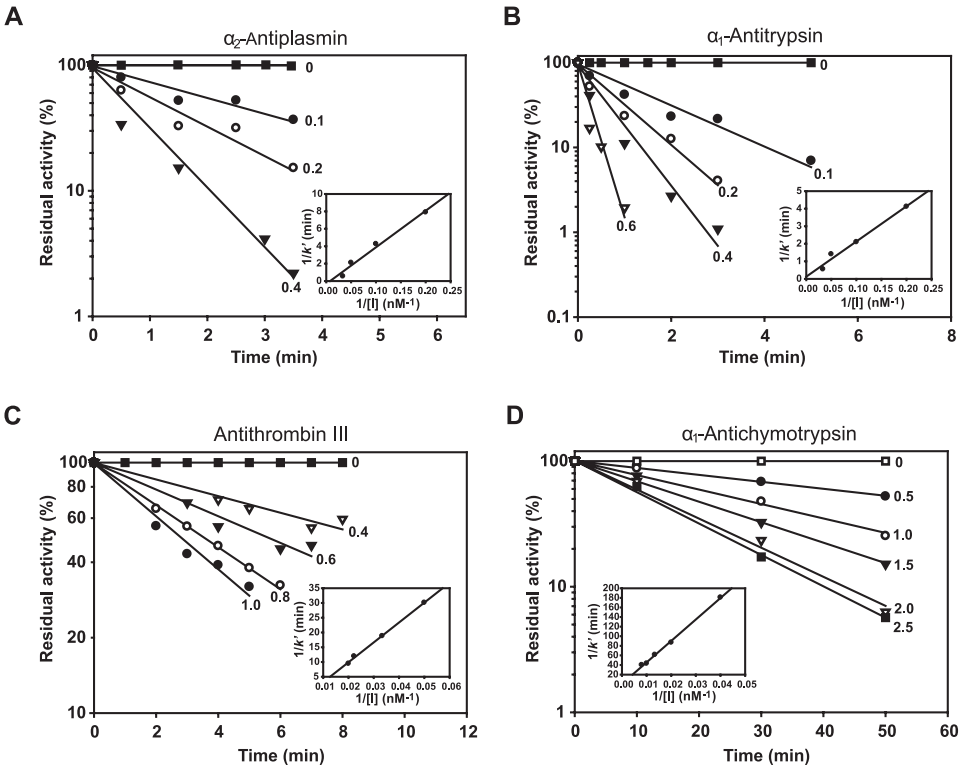

FIGURE 6. **Kinetics of inactivation of KLK14 by α_2-antiplasmin (*A*), α_1-antitrypsin (*B*), antithrombin III (*C*), and α_1-antichymotrypsin (*D*).** KLK14 (final concentration, 0.1 μM) was incubated with increasing concentrations of each serpin for various time intervals after which residual activity against QAR-AMC (0.2 mM final concentration) was measured. *A,* AP final concentration (μM): 0 (■), 0.1 (●), 0.2 (○), 0.4 (▼). *B,* AT final concentration (μM): 0 (■), 0.1 (●), 0.2 (○), 0.4 (▼), 0.6 (▽). *C,* ATIII final concentration (μM): 0 (■), 0.4 (▽), 0.6 (▲), 0.8 (○), 1.0 (●). *D,* ACT final concentration (μM): 0 (□), 0.5 (●), 1.0 (○), 1.5 (▼), 2.0 (▽), 2.5 (■). The *insets* show a double-reciprocal plot of the pseudo-first order rate constant (k') and the inhibitor concentration. The *line* drawn is a least squares fit of the experimental points. The equation of the line for AP is $Y = 42.02X + 0.32$ ($r = 0.981$); AT, $Y = 20.07X + 0.12$ ($r = 0.980$); ATIII, $Y = 673.7X + 3.57$ ($r = 0.998$); ACT, $Y = 5.54X + 2.0$ ($r = 0.996$). *r* is the Pearson correlation coefficient.

TABLE 3
Inhibition of KLK14 activity by serpins

Serpin	K_I	k_{+2}	k_{+2}/K_I
	μM	min^{-1}	$\mu M^{-1}\ min^{-1}$
Plasminogen activator inhibitor-1	ND[a]		
α_1-Antitrypsin	0.162	8.098	49.8
α_2-Antiplasmin	0.130	3.100	23.8
Antithrombin III	0.189	0.230	1.48
α_1-Antichymotrypsin	5.580	1.247	0.224

[a] ND indicates not determined.

trypsin-like and chymotrypsin-like serine proteases, respectively. In accord with our previous study (21), KLK14 displayed trypsin-like specificity with a greater catalytic efficiency for Arg *versus* Lys at the P1 position, as substrates with the highest k_{cat}/K_m values contain P1-Arg. The P1-Arg preference of KLK14 was further demonstrated by the location of KLK14 cleavage sites within intact proteins (Fig. 4; Table 5), all of which occurred C-terminal of Arg residues. However, in contrast to prior findings (19, 21), we could not ascribe chymotryptic-like specificity to KLK14 under the experimental conditions chosen, *i.e.* no hydrolytic activity against either AAPF-AMC or LLVY-AMC was detected. Possible explanations for this finding include the following: 1) the inherent incompatibility of the AMC-substrates used in our study with KLK14 (*i.e.* lack of P′ residues and the presence of unfavored residues at P2 and P3), 2) possible steric effects attributed to the interaction between AMC and the P1 amino acid (*e.g.* cleavage of a chymotrypsin-like chromogenic substrate, Ala-Pro-Tyr-*p*-nitroanilide, by KLK14 was reported in a previous study (19)), and 3) the final enzyme concentration used.

The P2 specificity of KLK14 was examined by comparing the k_{cat}/K_m values among substrate subgroups with invariable P1 and P3 residues as follows: 1) QAR-AMC, QGR-AMC, and QRR-AMC; 2) LKR-AMC, LRR-AMC, and LGR-AMC; and 3) GPR-AMC and GRR-AMC. As shown in Table 2, KLK14 exerts minimal, if any, catalytic activity toward substrates containing basic residues (*i.e.* Arg and Lys) at P2 and instead prefers relatively small, aliphatic amino acids (*i.e.* Gly and Ala) at this position. These results concur with those of our phage displayed library screening, because the vast majority of KLK14-selected pentapeptides contained P2 amino acids with aliphatic side chains (*i.e.* Gly, Ala, Val, and Leu), whereas none possessed basic P2 residues (21).

The P3 preference of KLK14 was assessed by examining k_{cat}/K_m values in substrate subgroups bearing the same P1 and P2 amino acids as follows: 1) VPR-AMC and GPR-AMC; 2) LGR-AMC, QGR-AMC, and GGR-AMC; and 3) QRR-AMC and LRR-AMC. Yet, unlike its relatively stringent P1 and modest P2 preferences, KLK14 possesses a lower specificity at P3. Specifically, the S3 subsite can accommodate a variety of amino acids, including basic residues and those with large and small aliphatic chains (21).

Regulation of KLK14 Activity

Serpins—Several extracellular inhibitory members of the serpin superfamily, namely α_1-antitrypsin (AT), α_1-antichymotrypsin (ACT), antithrombin III (ATIII), α_2-antiplasmin (AP), and plasminogen activator inhibitor-1 (PAI-1), were assayed for their inhibitory capacity against KLK14. Such inhibitory serpins behave as irreversible suicide substrate inhibitors and are cleaved by their protease targets at a scissile bond (P1-P1′) within their exposed reactive site loops (RSL), after which the interaction may proceed via the "inhibitory" or "substrate" pathway, resulting in complex formation or an inactive serpin and an active protease, respectively (34). The kinetics of inactivation of KLK14 activity in the presence of increasing serpin concentrations are displayed graphically in Fig. 6. The corresponding kinetic constants (K_I, k_{+2}) are listed in Table 3 and were calculated from the double-reciprocal plots of the pseudo-first order

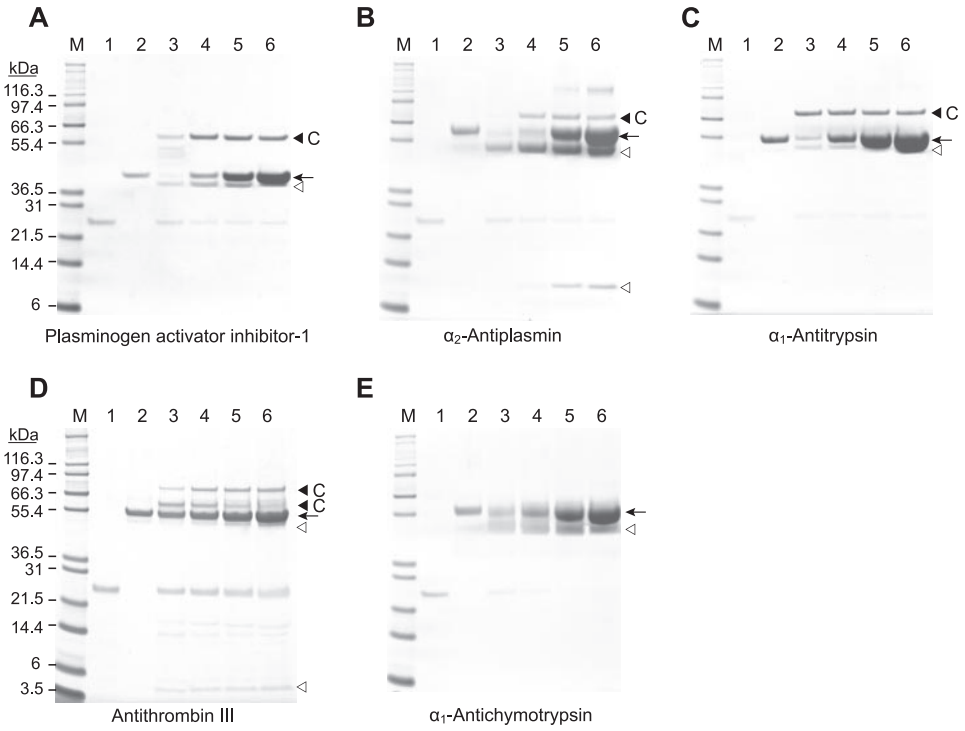

FIGURE 7. **SDS-PAGE analysis of the interaction between KLK14 and the serpins plasminogen activator inhibitor-1 (*A*), α_2-antiplasmin (*B*), α_1-antitrypsin (*C*), antithrombin III (*D*), and α_1-antichymotrypsin (*E*).** KLK14 was incubated at 1:1 (*lane 3*), 1:2 (*lane 4*), 1:5 (*lane 5*), and 1:10 (*lane 6*) molar ratios with different serpins at either 37 °C or at room temperature for time points specified under "Experimental Procedures." KLK14 and serpins incubated alone are shown in *lanes 1* and *2*, respectively. The mixtures were subsequently resolved by SDS-PAGE under reducing conditions, and the gels were stained with Coomassie Blue. Intact serpins are indicated with *arrows*. Complexes (▲; labeled *C*) were formed between KLK14 and all serpins, with the exception of α_1-antichymotrypsin. Interactions between KLK14 and all serpins also generated lower molecular weight fragments (△), indicative of substrate pathway contributions. *M*, molecular mass standards in kDa.

TABLE 4
Effect of ions on KLK14 activity

Ion[a]	Concentration tested[b]	Molar ratio (KLK14:ion)	Residual activity
	μM		%
Citrate	0.12	1:10	105
	1.2	1:100	109
	12	1:1000	113
	120	1:10000	131
Zn^{2+}	0.012	1:1	51
	0.12	1:10	5
	1.2	1:100	1
Mg^{2+}	1.2	1:100	85
Ca^{2+}	1.2	1:100	100
Na^{+}	1.2	1:100	100
K^{+}	1.2	1:100	100

[a] Zn^{2+} data correspond to incubation of KLK14 with $ZnCl_2$.
[b] KLK14 final concentration was 0.012 μM in all experiments.

rate constant k' *versus* inhibitor concentrations (Fig. 6, *insets*). Based on the apparent second order rate constants (k_{+2}/K_I) determined, the rank order for KLK14 inhibition by serpins from highest to lowest efficiency was AT > AP ⋙ ATIII ≫ ACT (Table 3). AT was ~2 times more effective than AP at KLK14 inactivation and 34- and 220-fold more efficient than ATIII and ACT, respectively. For instance, a 50% decrease in KLK14 activity was induced by AT (0.1 μM) in 1.2 min, by AP (0.1 μM) in 2.3 min, by ATIII (0.6 μM) in 5.7 min, and by ACT (1.0 μM) in 26 min. PAI-1 also inactivated KLK14; however, the reaction proceeded at a much higher rate than with other serpins; hence rate constant determination was not possible. For example, incubation of PAI-1 with KLK14 at a 1:1 molar ratio for 10 s at room temperature resulted in 100% inhibition of KLK14 activity. Thus, we speculate that PAI-1 is a more efficient inhibitor of KLK14 than AT.

Because the hallmark of the serpin inhibitory mechanism is the formation of a covalent complex between the serpin and its cognate protease (34), we visualized stable complexes between KLK14 and PAI-1, AP, AT, and ATIII but not ACT by SDS-PAGE under reducing conditions (Fig. 7). Single complexes of ~64, 90, and 77 kDa formed between KLK14 and PAI-1, AP, and AT, respectively (Fig. 7, *A–C*). However, two complexes of ~83 and 67 kDa formed between ATIII and KLK14 (Fig. 7*D*). The lower molecular weight complex may represent an interaction between ATIII and autodegradation fragment I of KLK14, which may retain partial serine protease activity, as discussed above. In addition to the inhibitory pathway, KLK14 also reacts with these serpins via the substrate pathway, at varying extents, as evidenced by the presence of lower molecular weight bands pertaining to cleaved serpin fragments (*i.e.* ~38 kDa for PAI-1 (Fig. 7*A*); ~50 and 10 kDa for AP (Fig. 7*B*); ~50 kDa for AT (Fig. 7*C*; ~53 and 4 kDa for ATIII (Fig. 7*D*); and ~50 kDa for ACT (Fig. 7*E*)). Based on our kinetic analysis, ACT is an inefficient inhibitor of KLK14 compared with the other serpins studied. A likely explanation may be that KLK14 reacts with ACT primarily via the substrate pathway, as reflected in Fig. 5*E* by the presence of a major ~50-kDa band, below that of intact ACT, which corresponds to cleaved ACT. Because of the minor contribution of the inhibitory pathway, the complex between KLK14 and ACT was not visualized under the given experimental conditions. Notably, other KLKs also react with serpins via the substrate pathway, for instance the interaction between KLK3/PSA and ACT (35) and of KLK5 with AP (27).

Ions—The relative hydrolytic activity of KLK14 against QAR-AMC in the presence of the anion citrate and the cations Zn^{2+}, Ca^{2+}, Mg^{2+}, Na^{+}, and K^{+} is shown in Table 4. The presence of citrate seemed to have an activating effect on KLK14 activity, particularly at higher citrate concentrations (12–120 μM). Citrate has analogous effects on KLK3 (36), KLK5 (33), and KLK6 (37) activity.

Among all cations tested, Zn^{2+} was able to inhibit KLK14 activity in a dose-dependent manner, with IC_{50} values of 15.3, 12.8, and 15.5 nM for $ZnCl_2$, $ZnSO_4$, $Zn(CH_3COO)_2$,

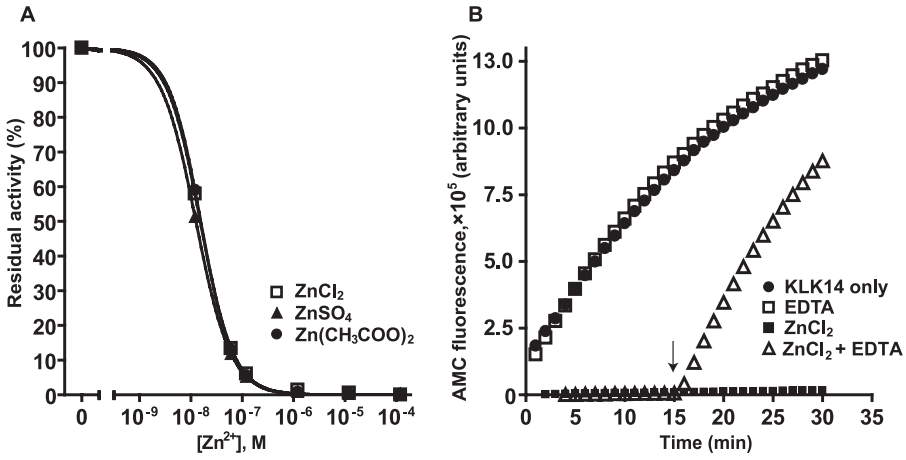

FIGURE 8. **Zinc inhibition of KLK14 activity (*A*) and its reversal by EDTA (*B*).** *A*, KLK14 (12 nM) was incubated with increasing concentrations (12, 60, 120, 1200, 12,000 and 120,000 nM) of $ZnCl_2$, $ZnSO_4$, and $Zn(CH_3COO)_2$ for 30 min after which residual KLK14 activity was measured against QAR-AMC. Zinc ions (Zn^{2+}) efficiently attenuate the activity of KLK14 with an average IC_{50} value of 1.46 nM. *B*, hydrolysis of QAR-AMC by KLK14 (12 nM) in the presence of: optimal buffer only (●), 1 mM EDTA (□), 1.2 mM $ZnCl_2$ (■), and 1.2 mM $ZnCl_2$ prior to and after the addition of 1 mM EDTA (▲). The *arrow* denotes the addition of 1 mM EDTA.

respectively (Fig. 8*A*; Table 4). Zinc inhibition was completely reversed by EDTA (Fig. 8*B*). In a similar fashion, Zn^{2+} also regulates the activity of KLK2 (38), KLK3 (39), KLK5 (33), KLK7 (40), and KLK8 (41). Mg^{2+} was also able to attenuate KLK14 activity, but to a much lesser extent, in contrast to its stimulatory effect on KLK8 activity (41). The remaining cations Ca^{2+}, Na^+, and K^+ had no significant effect on KLK14 activity up to concentrations of 1.2 mM, in contrast to the positive and negative influence of Na^+ on the activity of KLK3 (36, 42) and KLK6 (37), respectively.

Digestion of Potential Substrates by KLK14

ECM (fibronectin, laminin, and collagens I–IV) components, plasma proteins (fibrinogen, kininogen, plasminogen, and vitronectin), and insulin-like growth factor-binding proteins were highly susceptible to degradation by KLK14 *in vitro* (Figs. 9–11). In all cases, degradation was not observed in the absence of KLK14. In the presence of KLK14, however, all proteins were readily digested at varying efficiencies in a time-dependent manner, resulting in the generation of numerous proteolytic fragments (Figs. 9–11). The N-terminal sequence of several KLK14-generated fragments was identified, allowing for the determination of KLK14 cleavage sites within the intact molecules (Table 5).

Extracellular Matrix Components

Incubation of KLK14 with fibronectin resulted in the generation of several fragments, ranging in size from ~32 to 180 kDa (Fig. 9*A*). Based on the N-terminal sequence of fragments F1–F6, three major KLK14 cleavage sites were identified at Arg^{290}–Ala^{291}, Arg^{903}–Ser^{904}, and Arg^{2070}–His^{2071}, all of which lie between fibronectin-type domains, *i.e.* areas most susceptible to proteolysis (43) (Table 5). In terms of ligand-binding regions, the first site, Arg^{290}–Ala^{291}, lies between the first fibrin/heparin-binding region and the collagen/gelatin-binding region; the second site, Arg^{903}–Ser^{904}, is flanked by the collagen/gelatin-binding and cell-binding regions, whereas the third site occurs within "connecting strand 3," which links the second heparin-binding and fibrin-binding regions (43).

Both α and β chains of laminin were completely digested by KLK14 after a 4-h incubation period (Fig. 9*B*). In our previous study, we identified and confirmed one KLK14 cleavage site at Arg^{2421}–Asp^{2422} within the laminin α5 chain (21).

KLK14 was able to effectively process collagens I–IV in their denatured forms at 37 °C (Fig. 9, *C–F*), but not in their native conformations at 25 °C, as shown for collagen IV (Fig. 9*F*). KLK14 cleavage sites were identified within the collagen IV α2 chain at Arg^{1077}–Ala^{1078} and Arg^{1109}–Gly^{1110}. An additional putative cleavage site has also been discovered by our group in the less abundant α3 chain isoform at Arg^{833}–Gly^{834} (21).

Moreover, fluorescent conjugates of collagen I, collagen IV, and fibrinogen were also incubated with KLK14, and a progressive increase in fluorescence emission resulting from substrate degradation was observed (data not shown).

Plasma Proteins

KLK14 induced rapid and extensive degradation of the plasma proteins kininogen, plasminogen, fibrinogen, and vitronectin (Fig. 10). Proteolysis of low molecular weight kininogen (LMWK) by KLK14 over time yielded a number of kininogen fragments (Fig. 10*A*). One KLK14 cleavage site was revealed at Arg^{114}–Ser^{115} within the first of three cystatin-like domains that include LMWK (44), which harbor inhibitory activity against cysteine proteases. Based on our data, it was not possible to determine whether KLK14 can release lysyl-bradykinin (kallidin) from LMWK, a major consequence of KLK1 action (45).

KLK14 could completely digest fibrinogen chains Aα and Bβ after a 15-min incubation period. The γ chain, however, displayed higher resistance to KLK14-mediated proteolysis (Fig. 10*B*). The N-terminal sequence of several major degradation fragments, denoted G1–G4, indicated that KLK14 cleaved the Aα chain at Arg^{38}–Val^{39} and Arg^{510}–His^{511} and the Bβ chain at Arg^{44}–Gly^{45} (Table 5). Cleavage at the latter site by thrombin leads to the release of fibrinopeptide B, thereby unmasking a polymerization site that drives fibrin assembly (46). The same cleavage site within the Bβ chain was identified for KLK5 (27). Moreover, KLK4 (47) and KLK6 (48) have also been shown to digest fibrinogen, *in vitro*.

KLK14 digests plasminogen into three fragments of 30 (fragment P2), 50 (fragment P1), and 70 kDa, which result from cleavage at Lys^{96}–Lys^{97} and Arg^{549}–Lys^{550} (Fig. 10*C*; Table 5). Fragment P1 (Lys^{97}–Arg^{549}) corresponds to angiostatin4.5 ($AS_{4.5}$), an isoform of angiostatin consisting of the first four and 85% of the fifth kringle domain, which acts as a potent inhibitor of angiogen-

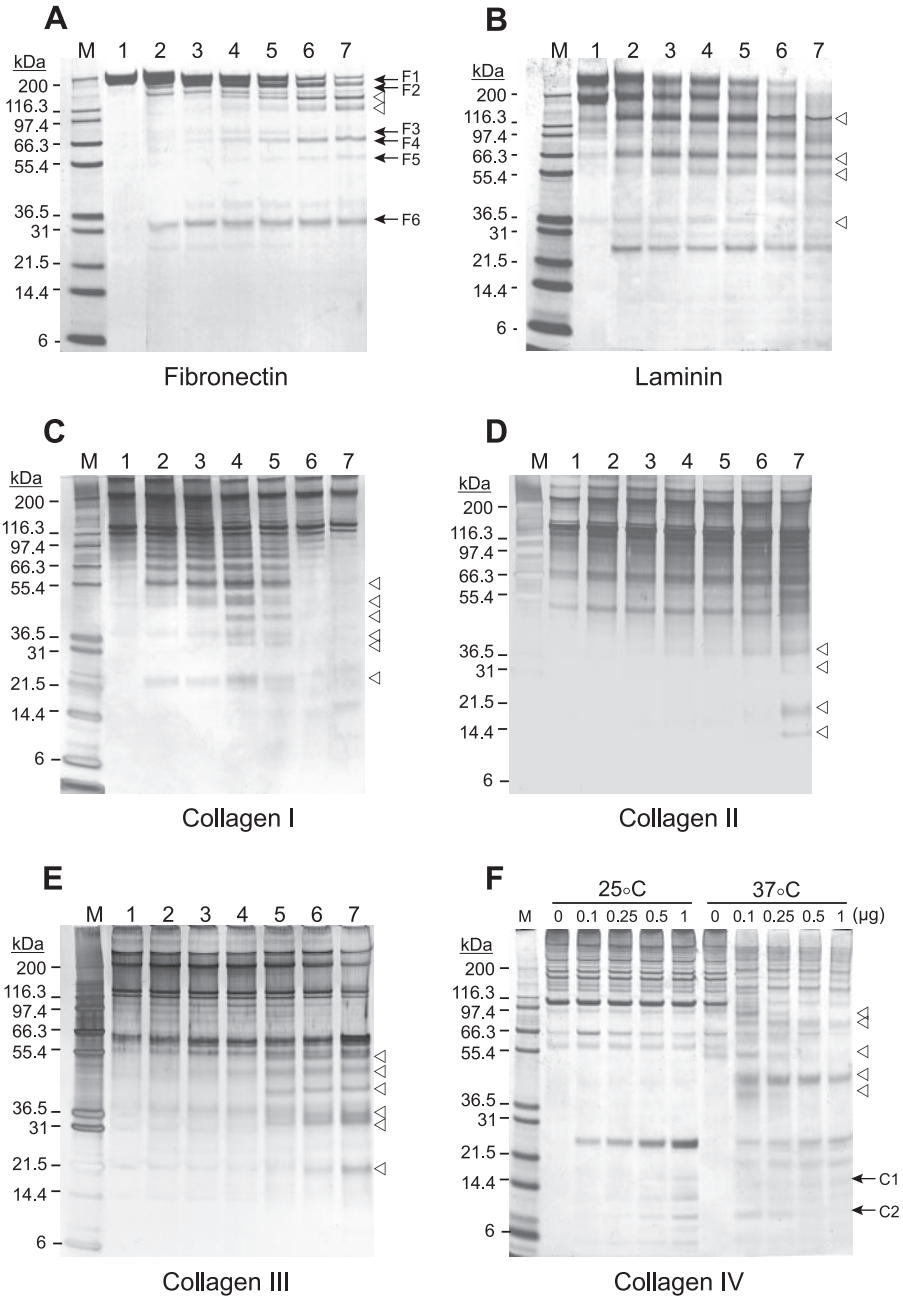

FIGURE 9. **KLK14-mediated degradation of the extracellular matrix proteins fibronectin (*A*), laminin (*B*), collagen I (*C*), collagen II (*D*), collagen III (*E*), and collagen IV (*F*).** KLK14 was incubated with 5 μg of fibronectin, laminin, and collagen IV and 2 μg of collagens I–III. *A–E*, *lane 1* represents each matrix protein incubated alone for 2 (in *A*) or 4 h (in *B–E*). *A, lanes 2–7* represent 0-, 5-, 15-, and 30-min and 1- and 2-h incubation periods, respectively. *B–E, lanes 2–7* correspond to 0-, 15-, and 30-min and 1-, 2-, and 4-h time points, respectively. *F,* increasing amounts of KLK14, shown in micrograms *above* each lane, were incubated with collagen IV for 8 h at either 25 or 37 °C. The mixtures were resolved by SDS-PAGE under reducing conditions, and the gels were stained with Coomassie Blue (*A, B,* and *F*) or silver (*C, D,* and *E*). Major KLK14-generated fragments are indicated by *open arrowheads*; *arrows*, and corresponding labels (*F1–6* and *C1–2*) denote fragments subjected to N-terminal sequence analysis (results are listed in Table 5). *M*, molecular mass standards in kDa.

esis (49). Fragment P2 (Lys^{550}–Asn^{810}) represents microplasmin, which consists of the remainder of the fifth kringle domain followed by the serine protease domain (50). Similarly, additional KLKs, including KLK3 (51), KLK5 (27), KLK6 (52), and KLK13 (53), can also generate angiostatin-like fragments from plasminogen *in vitro*.

Incubation of KLK14 with vitronectin resulted in the generation of several distinct fragments of ~60 and 20 kDa (Fig. 10*D*). N-terminal sequencing of fragment V2 revealed that KLK14 cleaves at peptide bond Arg^{64}–Gly^{65}, which is located directly within the cell attachment sequence (*i.e.* the integrin-binding site Arg^{64}–Gly^{65}–Asp^{66}) and adjacent to the C-terminal boundary of the somatomedin B domain (*i.e.* a binding site for plasminogen activator inhibitor-1 and of the urokinase receptor) (54). The N terminus of V3 indicated that a second KLK14 cleavage site exists at Arg^{197}–Asp^{198}, which lies within the middle of the molecule between its collagen and plasminogen-binding sites (54). KLK5 also processes vitronectin *in vitro*, but at cleavage sites distinct from those of KLK14 (27).

IGFBPs

KLK14 was able to completely digest IGFBP-2 and IGFBP-3 within 4-h and 15-min incubation periods, respectively (Fig. 11). Major fragments of ~28, 20, and 14 kDa were generated from IGFBP-2 (Fig. 11*A*), and products of ~28 and 14 kDa were obtained from IGFBP-3 (Fig. 11*B*). Although KLK14 cleavage sites within either IGFBP were not determined, the degradation products obtained are comparable with those generated by KLK2 (55), KLK3 (55, 56), and KLK5 (33). Given this, it may be inferred that KLK14, akin to other KLKs and many other proteases, may target IGFBPs within their middle linker region (57), which is flanked by areas that mediate binding to insulin-like growth factors I and II (IGF-1 and IGF-II) and may thereby decrease the affinity of IGFBPs for IGFs (58).

DISCUSSION

KLK14 is a relatively uncharacterized extracellular serine protease of the human tissue kallikrein family. Thus, its physiological targets, inhibitors, and role(s) are not well understood. The present data reveal a broad picture of KLK14 action, providing additional clues into this enzyme's selectivity for protein substrates, several regulatory mechanisms that control its activity, and potential biological and pathological consequences of KLK14 function.

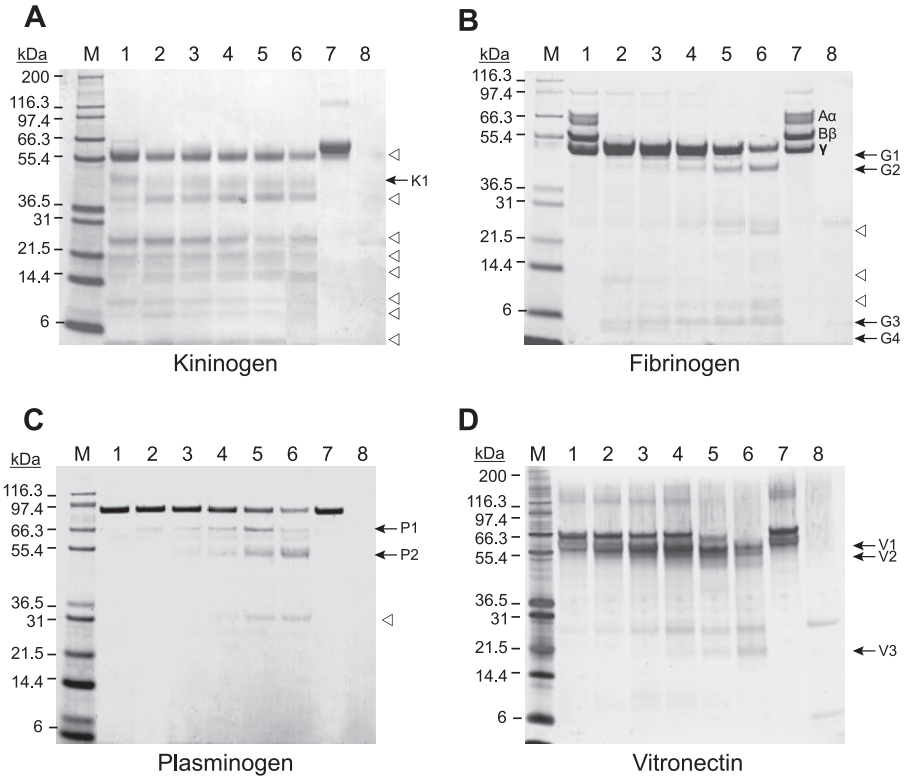

FIGURE 10. **KLK14-mediated degradation of the plasma proteins kininogen (*A*), fibrinogen (*B*), plasminogen (*C*), and vitronectin (*D*).** KLK14 was incubated with 5 μg of kininogen, 10 μg of fibrinogen and plasminogen, and 300 ng of vitronectin at 37 °C. *A–C, lanes 1–6* correspond to 0-, 15-, and 30-min and 1-, 2-, and 4-h time points, respectively. *D, lanes 1–6* represent 0-, 5-, 15-, and 30-min and 1- and 2-h incubation periods, respectively. *A–D, lanes 7* and *8*, plasma protein and KLK14, respectively, incubated alone for 4 (*A–C*) or 2 h (*D*). Reaction mixtures were resolved by reducing SDS-PAGE, and gels were stained with Coomassie Blue (*A–C*) or Silver (*D*). Major KLK14-generated fragments are indicated by *open arrowheads*; fragments subjected to N-terminal sequence analysis are indicated by *arrows* and labels on the *right* (results are listed in Table 5). *M*, molecular mass standards in kDa.

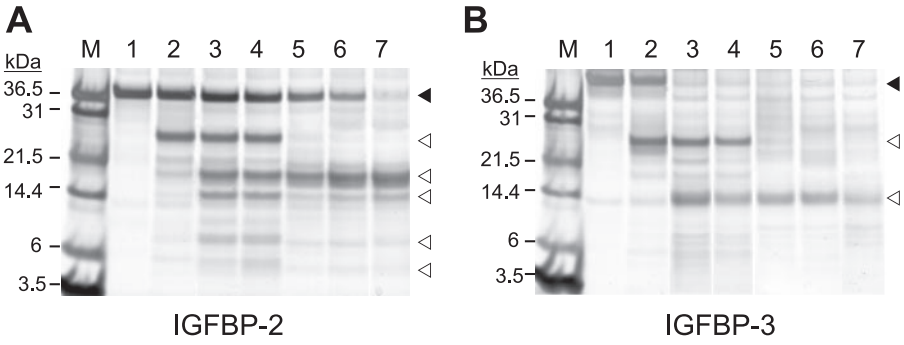

FIGURE 11. **Degradation of IGFBP2 and -3 by KLK14.** *A* and *B, lane 1* shows each IGFBP incubated alone for 4 h; *lanes 2–7* represent KLK14 (30 ng) incubated with IGFBPs (300 ng) for 0, 0.25, 0.5, 1, 2, and 4 h, respectively, at 37 °C. Intact IGFBPs are indicated by *solid arrowheads*; major KLK14-generated fragments are indicated by *open arrowheads*. *M*, molecular mass standards in kDa.

Multiple studies have investigated the expression of KLK14 at both the mRNA (7–9, 12, 16, 17) and protein level (10, 11, 14, 15) and concur that epithelial tissues of the normal and/or diseased breast, ovary, prostate, and skin are among the most abundant in KLK14. Our group was the first to detect and quantify the KLK14 protein in healthy and cancerous tissues and fluids via a sandwich-type ELISA consisting of mouse and rabbit polyclonal antisera, generated against recombinant KLK14 containing two fusion tags (10). Given the unexpectedly low KLK14 protein levels measured with this KLK14-ELISA, particularly in tissues and corresponding secretions that express abundant KLK14 mRNA (*e.g.* central nervous system-related tissues and fluids, including the brain, cerebellum, spinal cord and cerebrospinal fluid, respectively) (10), an additional survey of KLK14 content in tissues was required to clarify such discrepancies. Here, we describe the development of an improved KLK14-ELISA based on a monoclonal/polyclonal antibody configuration and re-examine KLK14 expression. As our new ELISA is generated against the native form of recombinant KLK14 (*i.e.* without fusion tags) and can effectively and specifically detect both recombinant mature and pro-KLK14, a more reliable and accurate measure of the total KLK14 content in the tissues, fluids, and cell lines was attained. KLK14 levels were highest in the normal skin/HaCaT keratinocyte cell line, breast/breast milk, and prostate/seminal plasma, in accord with prior studies. The concentrations of KLK14 in these tissues/fluids were comparable with those obtained by our previous ELISA (10). As evidenced by undetectable amounts of KLK14 in the majority of central nervous system tissues assayed (with the exception of minor levels in the medulla and spinal cord), our results confirm the previous observation that the KLK14 protein is generally absent in the central nervous system, despite the relative abundance of KLK14 transcripts in similar central nervous system tissues (7).

Numerous reports indicate that *KLK14* is dysregulated in malignancy (7, 9–11, 16, 17). In this study, we demonstrate that KLK14 is expressed in cancerous breast and ovarian tissue extracts and cell lines. We have shown previously that KLK14 is elevated in the serum of breast and ovarian cancer patients (10). This study is the first to report a significant elevation of KLK14 serum levels in prostate cancer patients compared with healthy males, which correlates with and may be attributable to the overexpression of *KLK14* transcripts observed in cancerous prostatic tissues *versus* normal counterparts (17). Thus, serum KLK14 might function as a complementary biomarker to PSA/KLK3 for prostatic diseases. KLK14-expressing breast cancer cell lines, MCF7 and MDA-MB-468, are derived from metastatic sites and likely rep-

TABLE 5
N-terminal sequence analysis of KLK14 degradation products and putative KLK14 cleavage sites

Fragment[a]	N-terminal sequence[b]	Cleavage site location
Collagen IV α2 chain (NP_001837)		
C1	(^{1077}R) ↓ AGLYGE	Collagen triple helix repeat
C2	(^{1109}R) ↓ GTTGIP	Collagen triple helix repeat
Fibronectin (NP_002017)		
F1/F2/F4/F5	(^{290}R) ↓ AAVYQP	Between 2 fibronectin type 1 domains
F3	(^{903}R) ↓ SDTVPS	Between 2 fibronectin type 3 domains
F6	(^{2070}R) ↓ HRPRPY	Between 2 fibronectin type 3 domains
Plasminogen (NP_000292)		
P1	(^{96}K) ↓ KVYLSE	C-terminal preactivation peptide
P2	(^{549}R) ↓ KLYDY	Kringle domain 5
Fibrinogen Aα chain (NP_068657)		
G1/G2	(^{38}R) ↓ VVERHQ	C-terminal to thrombin cleavage site
G3	(^{510}R) ↓ HRHPDE	N-terminal to the fibrinogen-related domain
Fibrinogen Bβ chain (NP_005132)		
G4	(^{44}R) ↓ GHRPLD	At thrombin cleavage site
Kininogen (NP_000884)		
K1	(^{114}R) ↓ SSTKFS	Cystatin-like 3 domain
Vitronectin (NP_000629)		
V1	NH_2-^{20}DQESCK	N terminus of mature vitronectin
V2	(^{64}R) ↓ GDVFTM	C terminus of somatomedin-B-like domain
V3	(^{197}R) ↓ DVWGIE	1st hemopexin-like repeat

[a] GenBank™ accession numbers are shown in parentheses.
[b] N-terminal sequence is preceded by the putative KLK cleavage site indicated by ↓ with the P1 amino acid in parentheses. Numbering starts from the initiator Met.

resent more aggressive forms of this disease; the ovarian cancer cells that produce KLK14 are of various grades and histotypes, including serous (OV-90), endometrioid (TOV112D; MDAH-2774), and clear cell (TOV-21G). In addition to breast and ovarian carcinoma, the clinical applicability of KLK14 expression in prostate cancer warrants further investigation. Taken together, the normal and/or diseased skin, breast, prostate, and ovary and their associated secretions likely represent the key tissues and fluids of KLK14 action.

Defining the specificity of an SP, *i.e.* its discrimination among substrates, allows for the identification of potential biological targets, a further understanding of its (patho)physiological role, and can direct the design of specific inhibitors. Although the S1 subsite is recognized as the primary determinant of substrate specificity in SP, the contribution of additional interactions between S4-S4′ and P4-P4′ can also be critical (59). To elucidate the primary and extend substrate specificity of KLK14, we have examined its optimal occupancy across S4-S4′ subsites based on the P4-P4′ residues within selected phage-displayed pentapeptides (21), fluorogenic AMC-peptides, and macromolecular substrates and inhibitors that efficiently interact with KLK14. We and others (19, 21) have shown previously that KLK14 manifests dual trypsin and chymotrypsin-like enzymatic specificity, with a rather strict preference for Arg and Tyr over Lys at the P1 position. However, as demonstrated in this study and by other independent investigators (19), the chymotrypsin-like activity of KLK14 cannot be readily assayed with commercially available chymotrypsin-like fluorogenic or chromogenic peptides using the same enzyme concentration as with trypsin-like peptides. Hence, it is likely that this activity requires prime side residues for optimal interactions as we have shown by phage display substrate (21) and by the ability of KLK14 to specifically cleave the ectodomain of desmoglein-1 at Tyr^{528}–Ser^{529} *in vitro*.[3] With respect to its extended specificity, we uncovered relatively modest amino acid preferences for KLK14 at S4-S2 and S1′-S4′. Although a variety of P4, P3, P2, P1′, P2′ and P3′ residues are accommodated by KLK14, 60% of all side chains on average contain either aliphatic (Leu, Val, and Gly) or hydroxyl groups (Thr and Ser). The most predominant residues at P4, P3, P2, P1′, P2′, and P3′ present in ~20% of all substrates are Thr, Gly, Leu, Ser, Ser, and Thr, respectively. A similar preference for P1′-Ser has also been documented for other KLKs, including KLK1 and KLK2 (60). With the exception of P2′-Tyr/Phe and P3′-Arg/Lys found in 9 and 11% of substrates, respectively, KLK14 generally does not favor hydrophobic or charged residues in its extended subsites. Notably, KLK14 exhibits selectively for Pro at P4′, as this residue was present in 30% of all substrates, indicating that P4′ may be an important contributor to KLK14 specificity.

Because the catalysis of peptide bonds by proteases is irreversible, several regulatory mechanisms have evolved to prevent unnecessary and potentially damaging protein degradation. In this study, we examined four regulatory mechanisms that control KLK14 activity as follows: 1) zymogen activation, 2) internal cleavage, 3) endogenous inhibitors, and 4) ions.

We examined pro-KLK14 activation by KLK5 and could not demonstrate the efficient conversion of pro-KLK14 into its active form via KLK5 action, even after a 3-h incubation at a 5:1 molar ratio. However, under similar conditions, Brattsand *et al.* (19) reported ~25% activation of pro-KLK14 by KLK5, which increased to ~80% after 24 h. Catalytic efficiency is often the main criterion used in the selection of an activating enzyme. Thus, if KLK5 could activate pro-KLK14 *in vivo*, the conversion reaction would occur at an exceedingly slow rate, which may not be biologically relevant. In actuality, KLK5 may be the physiological activator of pro-KLK2 and pro-KLK3 in prostatic tissues and fluids, a process that occurs within 10 min *in vitro* (33). The stringent P1-Arg specificity of KLK5 (27) may explain its differential activation capacity toward pro-KLK14 and pro-KLK2/KLK3, which require limited proteolysis after P1-Lys and P1-Arg residues, respectively, for maturation. Given the

[3] C. A. Borgoño, I. P. Michael, N. Komatsu, A. Jayakumar, R. Kapadia, G. L. Clayman, G. Sotiropoulou, and E. P. Diamandis, submitted for publication.

latter, candidate activators that co-localize with pro-KLK14 *in vivo* and possess a compatible specificity for P1-Lys may include KLK4 (47, 61), KLK8 (41), and membrane-type serine protease 1 (62).

Autodegradation leading to inactivation may represent another means by which the activity of KLK14 is regulated. Intermolecular KLK14-mediated processing events may begin with the proteolysis of the most solvent-accessible P1-Arg residues first, resulting in destabilization of KLK14 tertiary structure, which subsequently leads to its complete degradation. Similar cases of inactivation by internal cleavage have been made for a number of SP and KLK family members, including KLK2 (autolytic and/or KLK5-mediated cleavage at Arg^{125}–Leu^{126} and Arg^{168}–Ser^{169} (33, 63)), KLK3 (KLK5-mediated processing at Lys^{169}–Lys^{170} and Lys^{206}–Ser^{207} (33, 64)), KLK6 (autolysis at Arg^{80}–Glu^{81} (48, 65)), KLK11 (plasmin-mediated cleavage at Arg^{156}–Leu^{157} (66)), and KLK13 (autolytic processing at Arg^{114}–Ser^{115} (53)). Most internal cleavage sites occur at analogous locations within exposed surface loops, for instance the scissile bonds Arg^{168}–Ser^{169}, Lys^{169}–Lys^{170}, Arg^{156}–Leu^{157}, and Arg^{157}–Tyr^{158} of KLK2, KLK3, KLK11, and KLK14, respectively, all reside in the autolysis loop. Furthermore, clipped forms of KLK5 (67) and KLK7 (68) also exist *in vitro* and/or *in vivo*. In addition to abolishing catalytic activity, internal cleavage at specific sites may also alter SP specificity, as reported for thrombin (69).

Akin to many other KLKs (4), we found that KLK14 activity is inhibited by several serpins, including PAI-1, AT, AP, ATIII, and ACT, ranked in order of highest to lowest inhibitory efficiency. The P1-Arg preference of KLK14 and the presence of P1-Arg (PAI-1, AP, ATIII), P1-Met (AT), and P1-Leu (ACT) in the RSL of the serpins studied (34) may explain their relative inhibitory potencies against KLK14. As serpins play pivotal roles in the control of KLK activity in serum, amniotic fluid, breast milk, seminal plasma, and the prostate (4), the serpins studied may also represent *in vivo* inhibitors of KLK14 proteolytic function in similar physiological settings, with the exception of ACT, which displays exceedingly slow inhibitory kinetics against KLK14.

We have also demonstrated that KLK14 is positively and negatively regulated by citrate and zinc, respectively. Although these ions are secreted by a variety of cell types, a likely *in vivo* scenario for ion-mediated modulation of KLK14 activity may be within the prostate and seminal plasma, the latter of which contains 19–34 mM citrate and 1–4 mM Zn^{2+} (70), well above or within the range used in this study, respectively. Citrate also enhances the activity of other KLK family members (33, 36, 37) and has been shown to induce a conformational change in KLK3 leading to a more active configuration, likely via a thermodynamic solvent effect rather than a direct interaction (36). Zinc ions also exert an inhibitory effect on other KLKs (33, 38–41), and previous studies have defined the allosteric zinc-binding site, which is comprised of three His residues, within KLK3 (71) and KLK2 (38). However, only one corresponding His residue is present in KLK14, suggesting that zinc may bind and regulate KLK14 in a different manner than KLK2 and KLK3. As zinc inhibition is reversible by EDTA *in vitro*, and possibly by semenogelins within the seminal plasma *in vivo* (33), this mechanism is tightly regulated and highly dependent on the composition of the extracellular milieu. Furthermore, cations (*e.g.* zinc) have also been shown to alter the substrate specificity of a number of SP (*e.g.* prostasin) (72, 73); this effect on KLK14 may be worth examining in the future.

Based on its dysregulation in several malignancies and its *in vitro* substrate repertoire, KLK14 activity may be implicated in several aspects of tumor progression, including tumor growth, invasion, and angiogenesis. As with other KLKs (5) and proteases (74), the consequence of KLK14 action may be either stimulatory or inhibitory, depending on the cancer type and tumor microenvironment. Digestion of IGFBP-2 and IGFBP-3 by KLK14 may not only abolish the intrinsic tumor-suppressive functions of IGFBPs but may also cause the release of IGF-I and IGF-II, mitogenic peptides that stimulate the growth of normal and malignant cells (58). By cleaving vitronectin directly within its integrin-binding site (Arg^{64}–Gly^{65}), KLK14 may decrease integrin-mediated as well as urokinase receptor-mediated cell adhesion (75) and thereby enable tumor cell detachment. Via degradation of ECM components (*e.g.* collagen I–III and fibronectin) and proteins of vascular basement membranes (*e.g.* collagen IV and laminin), KLK14 may facilitate tumor cell invasion and metastasis. Yet, because KLK14 could only process collagens in their denatured and not native conformations *in vitro*, KLK14 likely acts sequential to collagenases (*i.e.* a subfamily of MMPs), which digest and thereby denature native collagens *in vivo* (76). Taken together, these tumor-promoting effects of KLK14 may explain why its levels are often associated with parameters of poor prognosis in breast and prostate cancers.

KLK14 may also exert tumor-suppressive functions, by unmasking cryptic cleavage sites within ECM and plasma proteins leading to liberation of fragments with angiostatic functions. For instance, KLK14 is able to generate $AS_{4.5}$ from plasminogen via cleavage at Lys^{96}–Lys^{97} and Arg^{549}–Lys^{550}, and may release a fibronectin fragment containing anastellin by cleavage at Arg^{290}–Ala^{291} and Arg^{903}–Ser^{904}. Both $AS_{4.5}$ and anastellin possess anti-angiogenic and/or anti-metastatic functions (49, 77). It remains to be investigated whether KLK14 can also cleave at cryptic sites within collagen IV and laminin (78), thereby releasing additional anti-angiogenic fragments. These indirect tumor-inhibitory activities of KLK14 may form the basis of its correlation with a favorable prognosis in ovarian cancer patients (9).

In addition to tumor progression, KLK14 may also potentiate the development of arthritic disease. This may occur directly, via degradation of collagenous (*e.g.* collagen II) and noncollagenous (*e.g.* matrilin-4 (21, 79)) structural molecules that form cartilage, and/or indirectly, by generating 29- and 45-kDa fibronectin fragments, via cleavage at Arg^{290}–Ala^{291} and Arg^{903}–Ser^{904}, that destroy cartilage by inducing the expression of MMPs and catabolic cytokines (80, 81) and by also mediating chronic pro-inflammatory responses via proteinase-activated receptor 2 (22), which is implicated in the pathology of arthritis (82). Recently we have immunohistochemically localized KLK14, and several other KLKs, within chondrocytes (83), which further supports our hypothesis that KLK14, and possi-

bly other KLKs, may contribute to the progression of arthritic diseases.

Accumulating evidence suggests that cross-talk exists among members of the KLK family and with other SP and MMP (5, 19). Data presented here suggest that KLK14 may interact with other serine proteases by indirectly regulating their activities. KLK14 cleaves vitronectin at Arg^{64}–Gly^{65} and releases the somatomedin B domain, the primary high affinity binding site for active PAI-1 (54). The interaction between vitronectin and PAI-1 is biologically important, as vitronectin not only stabilizes and increases the half-life of PAI-1 but also localizes its activity in plasma and tissues during several (patho)physiological processes, including fibrinolysis and tumor progression (54). Although the action of KLK14 releases the intact somatomedin B domain, which has been reported to stabilize PAI-1 (84), PAI-1 activity would no longer be localized, leading to the dysregulation of urokinase-mediated pericellular proteolysis.

Given the clinical data that link KLK14 expression to disease and the possible involvement of KLK14 in tumor progression and other (patho)physiological processes, the inhibition of KLK14 activity may represent a promising therapeutic strategy. To this end, we have already constructed highly specific recombinant serpins for KLK14 by replacing the RSL of AT and ACT with KLK14-selected pentapeptides from our phage-displayed library screen (85), which may be useful in future functional studies on KLK14 and in assessing its utility as a therapeutic target.

In summary, this study provides a number of functional inferences into the action of the novel serine protease, KLK14. Our data may help to direct future research needed to resolve the role(s) of KLK14 in normal and pathological states.

REFERENCES

1. Puente, X. S., Sanchez, L. M., Overall, C. M., and Lopez-Otin, C. (2003) *Nat. Rev. Genet.* **4,** 544–558
2. Rawlings, N. D., Morton, F. R., and Barrett, A. J. (2006) *Nucleic Acids Res.* **34,** D270–D272
3. Yousef, G. M., and Diamandis, E. P. (2001) *Endocr. Rev.* **22,** 184–204
4. Borgono, C. A., Michael, I. P., and Diamandis, E. P. (2004) *Mol. Cancer Res.* **2,** 257–280
5. Borgono, C. A., and Diamandis, E. P. (2004) *Nat. Rev. Cancer* **4,** 876–890
6. Diamandis, E. P. (1998) *Trends Endocrinol. Metab.* **9,** 310–316
7. Yousef, G. M., Magklara, A., Chang, A., Jung, K., Katsaros, D., and Diamandis, E. P. (2001) *Cancer Res.* **61,** 3425–3431
8. Hooper, J. D., Bui, L. T., Rae, F. K., Harvey, T. J., Myers, S. A., Ashworth, L. K., and Clements, J. A. (2001) *Genomics* **73,** 117–122
9. Yousef, G. M., Fracchioli, S., Scorilas, A., Borgono, C. A., Iskander, L., Puopolo, M., Massobrio, M., Diamandis, E. P., and Katsaros, D. (2003) *Am. J. Clin. Pathol.* **119,** 346–355
10. Borgono, C. A., Grass, L., Soosaipillai, A., Yousef, G. M., Petraki, C. D., Howarth, D. H., Fracchioli, S., Katsaros, D., and Diamandis, E. P. (2003) *Cancer Res.* **63,** 9032–9041
11. Fritzsche, F., Gansukh, T., Borgono, C. A., Burkhardt, M., Pahl, S., Mayordomo, E., Winzer, K. J., Weichert, W., Denkert, C., Jung, K., Stephan, C., Dietel, M., Diamandis, E. P., Dahl, E., and Kristiansen, G. (2006) *Br. J. Cancer* **94,** 540–547
12. Komatsu, N., Takata, M., Otsuki, N., Toyama, T., Ohka, R., Takehara, K., and Saijoh, K. (2003) *J. Investig. Dermatol.* **121,** 542–549
13. Stefansson, K., Brattsand, M., Ny, A., Glas, B., and Egelrud, T. (2006) *Biol. Chem.* **387,** 761–768
14. Komatsu, N., Tsai, B., Sidiropoulos, M., Saijoh, K., Levesque, M. A., Takehara, K., and Diamandis, E. P. (2006) *J. Investig. Dermatol.* **126,** 925–929
15. Komatsu, N., Saijoh, K., Sidiropoulos, M., Tsai, B., Levesque, M. A., Elliott, M. B., Takehara, K., and Diamandis, E. P. (2005) *J. Investig. Dermatol.* **125,** 1182–1189
16. Yousef, G. M., Borgono, C. A., Scorilas, A., Ponzone, R., Biglia, N., Iskander, L., Polymeris, M. E., Roagna, R., Sismondi, P., and Diamandis, E. P. (2002) *Br. J. Cancer* **87,** 1287–1293
17. Yousef, G. M., Stephan, C., Scorilas, A., Ellatif, M. A., Jung, K., Kristiansen, G., Jung, M., Polymeris, M. E., and Diamandis, E. P. (2003) *Prostate* **56,** 287–292
18. Komatsu, N., Suga, Y., Saijoh, K., Liu, A. C., Khan, S., Mizuno, Y., Ikeda, S., Wu, H. K., Jayakumar, A., Clayman, G. L., Shirasaki, F., Takehara, K., and Diamandis, E. P. (2006) *J. Investig. Dermatol.* **126,** 2338–2342
19. Brattsand, M., Stefansson, K., Lundh, C., Haasum, Y., and Egelrud, T. (2005) *J. Investig. Dermatol.* **124,** 198–203
20. Schechter, I., and Berger, A. (1967) *Biochem. Biophys. Res. Commun.* **27,** 157–162
21. Felber, L. M., Borgono, C. A., Cloutier, S. M., Kundig, C., Kishi, T., Ribeiro, C. J., Jichlinski, P., Gygi, C. M., Leisinger, H. J., Diamandis, E. P., and Deperthes, D. (2005) *Biol. Chem.* **386,** 291–298
22. Oikonomopoulou, K., Hansen, K. K., Saifeddine, M., Tea, I., Blaber, M., Blaber, S. I., Scarisbrick, I., Andrade-Gordon, P., Cottrell, G. S., Bunnett, N. W., Diamandis, E. P., and Hollenberg, M. D. (2006) *J. Biol. Chem.* **281,** 32095–32112
23. Luo, L. Y., Grass, L., Howarth, D. J., Thibault, P., Ong, H., and Diamandis, E. P. (2001) *Clin. Chem.* **47,** 237–246
24. Obiezu, C. V., Shan, S. J., Soosaipillai, A., Luo, L. Y., Grass, L., Sotiropoulou, G., Petraki, C. D., Papanastasiou, P. A., Levesque, M. A., and Diamandis, E. P. (2005) *Clin. Chem.* **51,** 1432–1442
25. Christopoulos, T. K., and Diamandis, E. P. (1992) *Anal. Chem.* **64,** 342–346
26. Borgono, C. A., Fracchioli, S., Yousef, G. M., Rigault de la Longrais, I. A., Luo, L. Y., Soosaipillai, A., Puopolo, M., Grass, L., Scorilas, A., Diamandis, E. P., and Katsaros, D. (2003) *Int. J. Cancer* **106,** 605–610
27. Michael, I. P., Sotiropoulou, G., Pampalakis, G., Magklara, A., Ghosh, M., Wasney, G., and Diamandis, E. P. (2005) *J. Biol. Chem.* **280,** 14628–14635
28. Kitz, R., and Wilson, I. B. (1962) *J. Biol. Chem.* **237,** 3245–3249
29. Schapira, M., Scott, C. F., and Colman, R. W. (1981) *Biochemistry* **20,** 2738–2743
30. Schapira, M., Scott, C. F., James, A., Silver, L. D., Kueppers, F., James, H. L., and Colman, R. W. (1982) *Biochemistry* **21,** 567–572
31. Edman, P. (1970) *Mol. Biol. Biochem. Biophys.* **8,** 211–255
32. Yousef, G. M., Polymeris, M. E., Grass, L., Soosaipillai, A., Chan, P. C., Scorilas, A., Borgono, C., Harbeck, N., Schmalfeldt, B., Dorn, J., Schmitt, M., and Diamandis, E. P. (2003) *Cancer Res.* **63,** 3958–3965
33. Michael, I. P., Pampalakis, G., Mikolajczyk, S. D., Malm, J., Sotiropoulou, G., and Diamandis, E. P. (2006) *J. Biol. Chem.* **281,** 12743–12750
34. Gettins, P. G. (2002) *Chem. Rev.* **102,** 4751–4804
35. Hsieh, M. C., and Cooperman, B. S. (2002) *Biochemistry* **41,** 2990–2997
36. Huang, X., Knoell, C. T., Frey, G., Hazegh-Azam, M., Tashjian, A. H., Jr., Hedstrom, L., Abeles, R. H., and Timasheff, S. N. (2001) *Biochemistry* **40,** 11734–11741
37. Angelo, P. F., Lima, A. R., Alves, F. M., Blaber, S. I., Scarisbrick, I. A., Blaber, M., Juliano, L., and Juliano, M. A. (2006) *J. Biol. Chem.* **281,** 3116–3126
38. Lovgren, J., Airas, K., and Lilja, H. (1999) *Eur. J. Biochem.* **262,** 781–789
39. Malm, J., Hellman, J., Hogg, P., and Lilja, H. (2000) *Prostate* **45,** 132–139
40. Franzke, C. W., Baici, A., Bartels, J., Christophers, E., and Wiedow, O. (1996) *J. Biol. Chem.* **271,** 21886–21890
41. Kishi, T., Cloutier, S. M., Kundig, C., Deperthes, D., and Diamandis, E. P. (2006) *Biol. Chem.* **387,** 723–731
42. Hsieh, M. C., and Cooperman, B. S. (2000) *Biochim. Biophys. Acta* **1481,** 75–87
43. Pankov, R., and Yamada, K. M. (2002) *J. Cell Sci.* **115,** 3861–3863
44. Salvesen, G., Parkes, C., Abrahamson, M., Grubb, A., and Barrett, A. J. (1986) *Biochem. J.* **234,** 429–434
45. Bhoola, K. D., Figueroa, C. D., and Worthy, K. (1992) *Pharmacol. Rev.* **44,** 1–80
46. Mosesson, M. W. (2005) *J. Thromb. Haemost.* **3,** 1894–1904
47. Obiezu, C. V., Michael, I. P., Levesque, M. A., and Diamandis, E. P. (2006)

Biol. Chem. **387,** 749–759
48. Magklara, A., Mellati, A. A., Wasney, G. A., Little, S. P., Sotiropoulou, G., Becker, G. W., and Diamandis, E. P. (2003) *Biochem. Biophys. Res. Commun.* **307,** 948–955
49. Soff, G. A. (2000) *Cancer Metastasis Rev.* **19,** 97–107
50. Wu, H. L., Shi, G. Y., Wohl, R. C., and Bender, M. L. (1987) *Proc. Natl. Acad. Sci. U. S. A.* **84,** 8793–8795
51. Heidtmann, H. H., Nettelbeck, D. M., Mingels, A., Jager, R., Welker, H. G., and Kontermann, R. E. (1999) *Br. J. Cancer* **81,** 1269–1273
52. Bayes, A., Tsetsenis, T., Ventura, S., Vendrell, J., Aviles, F. X., and Sotiropoulou, G. (2004) *Biol. Chem.* **385,** 517–524
53. Sotiropoulou, G., Rogakos, V., Tsetsenis, T., Pampalakis, G., Zafiropoulos, N., Simillides, G., Yiotakis, A., and Diamandis, E. P. (2003) *Oncol. Res.* **13,** 381–391
54. Schvartz, I., Seger, D., and Shaltiel, S. (1999) *Int. J. Biochem. Cell Biol.* **31,** 539–544
55. Rehault, S., Monget, P., Mazerbourg, S., Tremblay, R., Gutman, N., Gauthier, F., and Moreau, T. (2001) *Eur. J. Biochem.* **268,** 2960–2968
56. Cohen, P., Graves, H. C., Peehl, D. M., Kamarei, M., Giudice, L. C., and Rosenfeld, R. G. (1992) *J. Clin. Endocrinol. Metab.* **75,** 1046–1053
57. Bunn, R. C., and Fowlkes, J. L. (2003) *Trends Endocrinol. Metab.* **14,** 176–181
58. Firth, S. M., and Baxter, R. C. (2002) *Endocr. Rev.* **23,** 824–854
59. Hedstrom, L. (2002) *Chem. Rev.* **102,** 4501–4524
60. Bourgeois, L., Brillard-Bourdet, M., Deperthes, D., Juliano, M. A., Juliano, L., Tremblay, R. R., Dube, J. Y., and Gauthier, F. (1997) *J. Biol. Chem.* **272,** 29590–29595
61. Matsumura, M., Bhatt, A. S., Andress, D., Clegg, N., Takayama, T. K., Craik, C. S., and Nelson, P. S. (2005) *Prostate* **62,** 1–13
62. Takeuchi, T., Harris, J. L., Huang, W., Yan, K. W., Coughlin, S. R., and Craik, C. S. (2000) *J. Biol. Chem.* **275,** 26333–26342
63. Lovgren, J., Rajakoski, K., Karp, M., Lundwall, A., and Lilja, H. (1997) *Biochem. Biophys. Res. Commun.* **238,** 549–555
64. Watt, K. W., Lee, P. J., M'Timkulu, T., Chan, W. P., and Loor, R. (1986) *Proc. Natl. Acad. Sci. U. S. A.* **83,** 3166–3170
65. Bernett, M. J., Blaber, S. I., Scarisbrick, I. A., Dhanarajan, P., Thompson, S. M., and Blaber, M. (2002) *J. Biol. Chem.* **277,** 24562–24570
66. Luo, L. Y., Shan, S. J., Elliott, M. B., Soosaipillai, A., and Diamandis, E. P. (2006) *Clin. Cancer Res.* **12,** 742–750
67. Brattsand, M., and Egelrud, T. (1999) *J. Biol. Chem.* **274,** 30033–30040
68. Hansson, L., Stromqvist, M., Backman, A., Wallbrandt, P., Carlstein, A., and Egelrud, T. (1994) *J. Biol. Chem.* **269,** 19420–19426
69. Braun, P. J., Hofsteenge, J., Chang, J. Y., and Stone, S. R. (1988) *Thromb. Res.* **50,** 273–283
70. Kavanagh, J. P. (1985) *J. Reprod. Fertil.* **75,** 35–41
71. Villoutreix, B. O., Getzoff, E. D., and Griffin, J. H. (1994) *Protein Sci.* **3,** 2033–2044
72. Shipway, A., Danahay, H., Williams, J. A., Tully, D. C., Backes, B. J., and Harris, J. L. (2004) *Biochem. Biophys. Res. Commun.* **324,** 953–963
73. Page, M. J., MacGillivray, R. T., and Di Cera, E. (2005) *J. Thromb. Haemost.* **3,** 2401–2408
74. Egeblad, M., and Werb, Z. (2002) *Nat. Rev. Cancer* **2,** 161–174
75. Cherny, R. C., Honan, M. A., and Thiagarajan, P. (1993) *J. Biol. Chem.* **268,** 9725–9729
76. Coffey, J. W., Fiedler-Nagy, C., Georgiadis, A. G., and Salvador, R. A. (1976) *J. Biol. Chem.* **251,** 5280–5282
77. Yi, M., and Ruoslahti, E. (2001) *Proc. Natl. Acad. Sci. U. S. A.* **98,** 620–624
78. Bix, G., and Iozzo, R. V. (2005) *Trends Cell Biol.* **15,** 52–60
79. Klatt, A. R., Nitsche, D. P., Kobbe, B., Macht, M., Paulsson, M., and Wagener, R. (2001) *J. Biol. Chem.* **276,** 17267–17275
80. Homandberg, G. A., and Hui, F. (1996) *Arch. Biochem. Biophys.* **334,** 325–331
81. Stanton, H., Ung, L., and Fosang, A. J. (2002) *Biochem. J.* **364,** 181–190
82. Ferrell, W. R., Lockhart, J. C., Kelso, E. B., Dunning, L., Plevin, R., Meek, S. E., Smith, A. J., Hunter, G. D., McLean, J. S., McGarry, F., Ramage, R., Jiang, L., Kanke, T., and Kawagoe, J. (2003) *J. Clin. Investig.* **111,** 35–41
83. Petraki, C. D., Papanastasiou, P. A., Karavana, V. N., and Diamandis, E. P. (2006) *Biol. Chem.* **387,** 653–663
84. Seiffert, D., and Loskutoff, D. J. (1991) *J. Biol. Chem.* **266,** 2824–2830
85. Felber, L. M., Kundig, C., Borgono, C. A., Chagas, J. R., Tasinato, A., Jichlinski, P., Gygi, C. M., Leisinger, H. J., Diamandis, E. P., Deperthes, D., and Cloutier, S. M. (2006) *FEBS J.* **273,** 2505–2514
86. Huber, R., Kukla, D., Bode, W., Schwager, P., Bartels, K., Deisenhofer, J., and Steigemann, W. (1974) *J. Mol. Biol.* **89,** 73–101

Expression and Functional Characterization of the Cancer-related Serine Protease, Human Tissue Kallikrein 14

Carla A. Borgoño, Iacovos P. Michael, Julie L. V. Shaw, Liu-Ying Luo, Manik C. Ghosh, Antoninus Soosaipillai, Linda Grass, Dionyssios Katsaros and Eleftherios P. Diamandis

J. Biol. Chem. 2007, 282:2405-2422.
doi: 10.1074/jbc.M608348200 originally published online November 16, 2006
